Chemical Physics 71 (1982) 417–441
North-Holland Publishing Company

SUPERFINE AND HYPERFINE STRUCTURES IN THE ν_3 BAND OF $^{32}SF_6$ ‡

Jacques BORDÉ and Christian J. BORDÉ
Laboratoire de Physique des Lasers, Associé au CNRS No. 282, Université Paris-Nord, Avenue J.B. Clément, 93430 Villetaneuse, France

Received 28 April 1982

We present a first detailed account of our theoretical approach to reproduce observed superfine and hyperfine structures in the ν_3 band of SF_6 and we display various observed and calculated patterns of superfine clusters exhibiting hyperfine effects. The main operators of the hamiltonian are derived and the associated constants are related to molecular parameters. We show that, owing to the off-diagonal terms in the hyperfine hamiltonian, a mixing occurs between vibration–rotation states with different point-group symmetry species. As a consequence, superfine and hyperfine structures have to be considered simultaneously and hyperfine hamiltonian matrices connecting several vibration–rotation states need to be diagonalized to reproduce the spectra. We analyse in greater detail a few typical examples from which several molecular constants have been determined (e.g. t_{044}, c_d). For the first time, the sign of c_d is obtained. Also an effective change, Δc_d, is found between upper and lower levels which can be readily interpreted as a manifestation of the tensor spin–vibration interaction.

1. Introduction

During the past fifteen years, the resolving power of infrared spectroscopy has been multiplied by a factor over 10^6 from the gigahertz to the kilohertz level. Favourite test molecules for this research have been spherical tops such as CH_4 [1], OsO_4 and especially SF_6 [2–13], partly because of many favourable coincidences with laser lines but also because of the beauty of the formalism developed for these molecules and finally because of the boost given to their study by laser isotope separation programs. For these molecules the considerable progress in resolution which has been achieved, has revealed new structures of tremendous richness and complexity. This progress is illustrated by fig. 1 where spectra of the ν_3 band of SF_6 at increasing levels of resolution are displayed. At the lowest resolution (top of the figure) we find the band envelope recorded by Brunet and Perez with a Girard grid spectrometer having a 0.07 cm^{-1} resolution [3]. This stage only shows the existence of P, Q and R branches as well as the presence of many hot bands. The next step, which requires either semiconductor diode lasers or Fourier transform spectroscopy exhibits the tensor fine structure of each J manifold [4]. This tensor structure is only partly resolved owing to the Doppler width limitation which leaves many clusters of lines unresolved. To go further and resolve the structure of these clusters (superfine structure) sub-Doppler methods such as saturation spectroscopy are required. Superfine splittings have been observed since the very beginning of saturation spectroscopy and the $Q(38)F_2^0E^0F_1^0$ triplet in coincidence with the P(16) CO_2 laser line is the most familiar example since it was first resolved in 1969 [5]. The fact that this triplet was not published in the open literature until 1977 [6,7] shows clearly enough the lack of appreciation of the importance of these structures over that period. The underlying physics was not understood until the work of Harter and Patterson [14] following earlier ideas of Dorney and Watson [15]. They showed that clusters had their origin in a spontaneous breaking of the point-group symmetry T_d or O_h into a lower symmetry (C_3 or C_4 subgroups). Since there are 6 (respectively 8) equiv-

‡ Work supported in part by DRET, by the Laboratoire de Physique Moléculaire et d'Optique Atmosphérique, Orsay, France, and by the Laboratoire de Spectroscopie Moléculaire, Université Pierre et Marie Curie, Paris, France.

0301-0104/82/0000–0000/$ 02.75

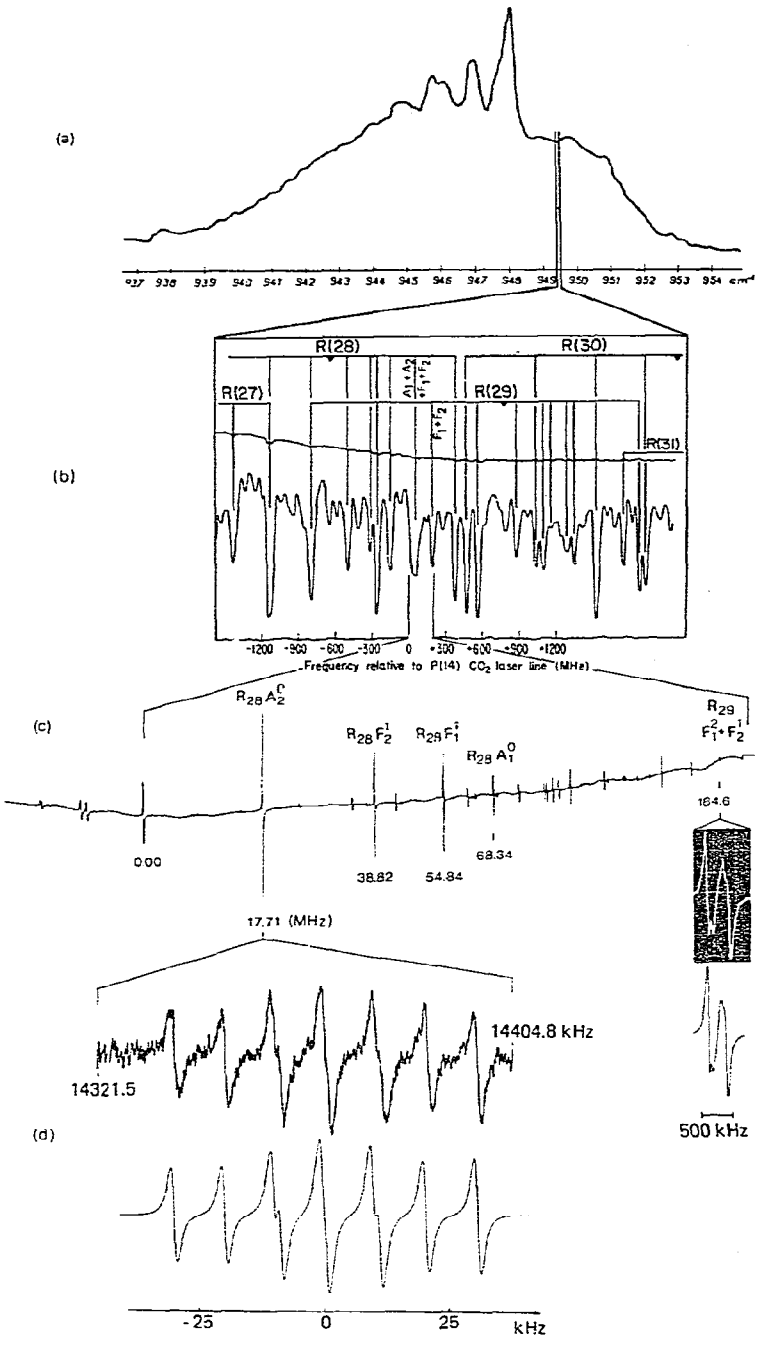

Fig. 1. Structure of the ν_3 band of $^{32}SF_6$ at increasing levels of resolution: (a) Room-temperature band-contour of the PQR type obtained with a Girard grid spectrometer [3]. (b) Doppler-limited semiconductor diode laser spectrum exhibiting the tensor fine structure of J-manifolds and unresolved clusters [4]. (c) Part of saturation spectrum obtained with a free-running waveguide CO_2 laser (resolution ≈20–40 kHz [7,8]) and exhibiting the superfine structures of a trigonal cluster (R(28) $A_2^0F_2^1F_1^1A_1^0$) and of a tetragonal cluster (R(29) $F_1^2F_2^1$). (d) Saturation spectrum obtained with a frequency-controlled laser spectrometer (resolution ≈1 kHz [10,13]) exhibiting the hyperfine structure of the R(28) A_2^0 line and the splittings between $I = 1$ and $I = 3$ components. The absolute frequency of the R(28) A_2^0 line center is 28.464 691 306 THz [11].

alent C_4 (respectively C_3) axes of rotation, this results in a 6 or 8-fold remaining degeneracy. The tunneling between these equivalent axes of rotation (tumbling motion) tends to restore the original symmetry and splits the clusters into individual components which are labeled by representations of the original group. The corresponding superfine structures are doublets, triplets or quadruplets with well-defined patterns that will be illustrated in this paper (e.g. the quadruplet R(28) $A_2^0F_2^1F_1^1A_1^0$ in fig. 1). At the highest resolution (with a frequency-controlled laser spectrometer) vibration–rotation lines exhibit their magnetic hyperfine structure [1,2,9,10] as illustrated with the R(28) A_2^0 line of fig. 1. As we shall see in greater detail, these magnetic hyperfine splittings occur because the nuclear spins are sensing magnetic fields of various origins in the molecule. The major surprise in these spectra came from unexpected crossover resonances which have now been successfully interpreted as forbidden lines coming from a mixture of states by off-diagonal contributions of the hyperfine hamiltonian [2,12]. The hyperfine interactions violate the molecular point-group symmetry species of vibration–rotation states and respect only the Pauli principle. The breakdown of the molecular point-group produces spectacular structures and splittings (such as F_{1u}–F_{1g} or A_{1u}–A_{1g} splittings) and the detailed study of these new effects is the main subject-matter of this paper. Let us emphasize that, as a consequence of these mixings, superfine and hyperfine structures cannot be treated separately.

The kilohertz resolution illustrated in fig. 1 in the case of the R(28) A_2^0 line has recently been extended to the full 600 MHz tuning range provided by CO_2 waveguide lasers around each CO_2 laser line [13]. As a result, a great number of hyperfine and superhyperfine structures have been recorded and are presently being analysed. In the present paper we shall limit ourselves to basic considerations and to a presentation of the methods and of the formulae which have led to the results published in ref. [12]. Only a few early examples, comprising those given in ref. [12], will be discussed here, mainly for the sake of illustrating various situations encountered in the spectra.

In 1978 a paper by Itano [16] appeared on the calculation of hyperfine structures in tetrahedral molecules and we extended his treatment from T_d molecules to the case of an O_h molecule such as SF_6. Also in 1979, a paper by Michelot et al. [17] gave the formal expressions of possible hyperfine operators and their matrix elements in spherical-top molecules. Along the presentation of our calculation, we shall make extensive use of the material contained in these two papers and this paper can somehow be considered as a link between the two approaches.

It is also obvious that many other previous works on nuclear hyperfine interactions in molecules have inspired us and a good review of these theoretical and experimental results has been published by Dymanus [18]. Here we shall strictly focus on the ν_3 band of SF_6: in section 2, we give details on the group-theory material that we use; in section 3, we establish the hamiltonian operators responsible for the splittings under study and finally, in section 4, we display and analyse several examples of hyperfine effects in fine and superfine structures.

2. Group theory and general conventions

We shall follow the basic idea [19,20] that the invariance group of a quasi-rigid molecule is $^LO(3) \times G$ when no external field is applied; $^LO(3)$ is the full rotation group of the space-fixed frame (SFF) and G is the point group of the equilibrium configuration. In the case of SF_6, G is the group O_h and we shall make ours the numbering of the nuclei specified in ref. [17] as well as the definitions of the operations and of the irreducible representation matrices described in refs. [21,22] ‡. These are consistent with the exhaustive work on the Racah algebra of the point group O published by Griffith [23], so that we shall be able to use his tables of V, W and X coefficients (analogous to the Wigner $3j$, $6j$ and $9j$ symbols respectively). The point group O_h will often be considered as a subgroup of the full rotation group $^MO(3)$ of the molecule-fixed frame (MFF) and it will be convenient to introduce irreducible representations (IRs) of $^MO(3)$ which are oriented with regard to this subgroup [24]: the IRs of $^LO(3)$ will be the standard ones, with spherical basis and active rotation matrices [25], and will be labeled

‡ In ref. [21], one should read $\sqrt{3}$ instead of 3 in the matrix $^ED(C_3)$.

with J_τ, where τ is the parity character g or u. Irreducible tensors and IRs of $^{L}O(3) \times G$ will then be specified by (J_τ, C) or $(J_\tau, J'_{\tau'}, nC)$ if we deal with quantities which are also tensors in $^{L}O(3) \times {}^{M}O(3)$ (rotational wavefunctions are such quantities for which we have $J_\tau \equiv J'_{\tau'}$: $\Psi_{M\sigma}^{(J_\tau, J_\tau nC)}$ or $|J_\tau M, J_\tau nC\sigma\rangle$).

The molecular wavefunctions can be written as a product of two wavefunctions: the rovibrational wavefunction Ψ_{VR} and the nuclear spin wavefunction Ψ_{NS} which will both be, separately, irreducible tensors. The irreducible tensors Ψ_{NS} are unambiguously labeled with the total nuclear spin I and the O_h symmetry species C_S; the correspondence between I and C_S has been worked out independently in refs. [26] and [43] and the explicit expressions of the components $\Psi_{NSM_I\sigma}^{(g, C_S)}$ or $|I_g M_I C_S \sigma\rangle$, as linear combinations of the functions $\Pi_{i=1,6}|\frac{1}{2}, m_i\rangle$ can be found in ref. [17].

We shall also use the classification proposed by Berger [27] for energy levels: the symmetry species of Ψ_{VR} will be $(J_\tau, J'_{\tau'}, nC)$, where $J'_{\tau'} \equiv J_\tau$ in the ground vibrational state and $J'_{\tau'} = R_{\tau \times u}$ in the $\upsilon_3 = 1$ state; Ψ_{VR} will then be written as $|J_\tau M, R_{\tau'} nC_R \sigma, \upsilon_3, \alpha\rangle$, where α gathers all the unspecified quantum numbers. The molecular wavefunction must satisfy the Pauli principle and only combinations of $\Psi_{NS}\Psi_{VR}$ which are of symmetry species A_{2u} must be considered. Akin to that coupling in the point group O_h, we shall couple Ψ_{NS} and Ψ_{VR} in $^{L}O(3)$ to obtain the total angular momentum $F = I + J$. Finally a total molecular state vector will be written as

$$|(J_\tau I_g) F M_F; (R_{\tau'} nC_R C_S)\, A_{2u}; \upsilon_3, \alpha\rangle .$$

Operators will also be symmetry-adapted; vibration–rotation operators T_{VR} and nuclear spin operators T_{NS} can be separately written as irreducible tensors and matched to give a totally invariant hamiltonian of symmetry species $(0_g, A_{1g})$; in order to build totally invariant operators or Pauli-satisfying wavefunctions; one just needs to apply standard rules for Kronecker products of IRs. Once we have quantities written as irreducible tensors, we can use all the power of Racah algebra to perform the couplings and compute matrix elements:

(I) The matrix elements of an operator $T_{M_2\sigma_2}^{(J_2, C_2)}$ satisfies the Wigner–Eckart theorem:

$$\langle J_{\tau_1}, M_1, n_1, C_1, \sigma_1 | T_{M_2,\sigma_2}^{(J_{\tau_2}, C_2)} | J_{\tau_3}, M_3, n_3, C_3, \sigma_3 \rangle$$

$$= (-1)^{J_{\tau_1} - M_1} \begin{pmatrix} J_{\tau_1} & J_{\tau_2} & J_{\tau_3} \\ -M_1 & M_2 & M_3 \end{pmatrix} V \begin{pmatrix} C_1 & C_2 & C_3 \\ \sigma_1 & \sigma_2 & \sigma_3 \end{pmatrix} \langle J_{\tau_1} n_1 C_1 \| T^{(J_{\tau_2}, C_2)} \| J_{\tau_3} n_3 C_3 \rangle . \tag{1}$$

This is consistent with eq. (14) of ref. [17] since, for O_h, covariant and contravariant components are identical. (To make formulae less cumbersome, from now on we shall omit τ whenever possible, e.g. in $3\text{-}j$ symbols which are $SO(3)$ $3\text{-}j$ symbols if $\tau_1 \times \tau_2 \times \tau_3 = g$ and zero if not.)

(II) The coupling of two irreducible tensors $T^{(J_1\tau_1, C_1)}$ and $T^{(J_2\tau_2, C_2)}$ will give irreducible tensors (J_τ, C) according to

$$[T^{(J_1, C_1)} \times T^{(J_2, C_2)}]_{M,\sigma}^{(J,C)} = \{(2J+1)[C]\}^{1/2} (-1)^{J_1 - J_2 + M}$$

$$\times \sum_{\substack{M_1 M_2 \\ \sigma_1 \sigma_2}} \begin{pmatrix} J_1 & J_2 & J \\ M_1 & M_2 & -M \end{pmatrix} V \begin{pmatrix} C_1 & C_2 & C \\ \sigma_1 & \sigma_2 & \sigma \end{pmatrix} T_{M_1\sigma_1}^{(J_1, C_1)} T_{M_2\sigma_2}^{(J_2, C_2)} . \tag{2}$$

In the case of wavefunctions, we shall take in the above formula $J_{2\tau_2} = I_g$, $J_\tau = F_{\tau_1}$ and $C = A_{2u}$; in the case of two operators H_{VR} and H_{NS} leading to a total hamiltonian operator, one must have $J_\tau = 0_g$ and $C = A_{1g}$ which implies $J_{1\tau_1} \equiv J_{2\tau_2}$ and $C_1 \equiv C_2$; in this case, (2) is related to the double scalar product as mentioned in ref. [16]:

$$H_{VR}^{(J_\tau, C)} : H_{NS}^{(J_\tau, C)} = (-1)^J [(2J+1)[C]]^{1/2} [H_{VR}^{(J_\tau, C)} \times H_{NS}^{(J_\tau, C)}]^{(0_g, A_{1g})} . \tag{3}$$

(III) The matrix elements of such an invariant operator in the coupled basis are given by

$$\langle (JI)FM_F; (RnC_R C_S)\,A_{2u}; \upsilon_3\alpha | [H_{VR}^{(J'',C'')} \times H_{NS}^{(J'',C'')}]^{(0_g,A_{1g})} | (J'I')F'M'_F; (R'n'C'_R C'_S)\,A_{2u}; \upsilon'_3\alpha' \rangle$$

$$= \delta_{FF'}\delta_{M_F M'_F} \frac{(-1)^{A_{2u}+C''+C_R+C'_S+J''+F+I+J'}}{[C'']^{1/2}[2J''+1]^{1/2}} \begin{Bmatrix} C'_R & C'_S & A_{2u} \\ C_S & C_R & C'' \end{Bmatrix} \begin{Bmatrix} I' & J' & F \\ J & I & J'' \end{Bmatrix}$$

$$\times \langle J, RnC_R\upsilon_3\alpha \| H_{VR}^{(J'',C'')} \| J', R'n'C'_R\upsilon'_3\alpha' \rangle \langle I, C_S \| H_{NS}^{(J'',C'')} \| I'C'_S \rangle . \tag{4}$$

The reduced matrix elements of nuclear spin operators will be calculated by eq. (1); the reduced matrix elements of rovibrational operators can be found in the abundant literature on spherical-top molecules [29]; an important discussion on the phase of these reduced matrix elements is developed in ref. [30]. If the operator $H_{VR}^{(J'',C'')}$ can be written as $H_{VR}^{(J'',R''n''C'')}$, its reduced matrix elements are given by [31]:

$$\langle J, RnC_R\upsilon_3\alpha \| H_{VR}^{(J'',R''n''C'')} \| J', R'n'C'_R\upsilon'_3\alpha' \rangle$$

$$= (-1)^R K_{nC\,n''C''}^{R\quad R''\quad R'} \langle J, R\alpha \| H_{VR}^{(J'',R'')} \| J', R'\alpha' \rangle . \tag{5}$$

In the course of this work, we have thus needed isoscalar coefficients $K_{n_1C_1\ nC\ n_2C_2}^{R\quad k\quad R}$ whose values are not reported in the literature when $n_1C_1 \neq n_2C_2$ and we give in the appendix the values of the relevant coefficients necessary to understand the examples presented in section 4. Now that we have defined the mathematical tool that we want to use and which is completely consistent with the analogous formulae given in ref. [17], we want to write down the hyperfine operators, explicitly, as in ref. [16], and transform them to expressions suitable for that tool.

3. The vibration–rotation and hyperfine hamiltonians

The effective molecular hamiltonian that we use is the sum of a vibration–rotation hamiltonian and of a nuclear hyperfine hamiltonian. The vibration–rotation part is the usual contact-transformed Darling–Dennison expansion which has been described extensively in the literature for the ground state and for a triply degenerate excited state [28–30]. The nuclear spin interaction hamiltonian will be derived in a manner similar to that followed by Itano [16] for T_d molecules; we shall obtain expressions consistent with the effective hyperfine hamiltonian deduced from the real hamiltonian through one electronic contact transformation [30]. Actually it is convenient to split the effective hamiltonian into three parts:

$$H = H_{VR}^0 + H_{VR} + H_{hyp} , \tag{6}$$

where H_{VR}^0 represents our "zeroth-order" vibration–rotation hamiltonian for which we assume that we know the eigenvalues E_{VR}^0 and in addition we shall keep in H_{VR}^0 only terms that do not lift the spherical degeneracy: all states with the same J, R, l_3 and υ_3 belong to the same E_{VR}^0. We shall then take this E_{VR}^0 as our zero energy since we are only interested in narrow spectral structures, within a given R-manifold. For the spectra that we want to reproduce, all terms which do not split the substates of a given R-manifold would result in a mere translation of the spectrum and we suppose that they are gathered in H_{VR}^0.

3.1. The vibration–rotation hamiltonian H_{VR}

H_{VR} gathers all the vibration–rotation (VR) terms that we need in order to calculate a correct pattern of VR levels. It is easy to calculate this pattern in the $\upsilon_3 = 1$ state: the tensorial splittings between VR lines have been fitted with the spectroscopic parameters given in ref. [2] and with off-diagonal corrections; the hamiltonian constants that can be derived from this fit yield a tensorial splitting of levels in the $\upsilon_3 = 1$ state only, so that the pattern of levels can be taken identical to the pattern of VR lines. Practically, this pattern can be calculated satisfac-

torily for our purpose with the second-order fourth-rank tensor T_{224} (in Robiette's notation [32]) and off-diagonal corrections in R only; the hamiltonian constant t_{224} is related to the spectroscopic parameter g ($t_{224} = -2g(7/12)^{1/2}$) and is equal to 1125.58 kHz.

In the ground state, the operator T_{224} has no non-zero matrix elements and the first operator in the hamiltonian expansion which gives rise to a tensorial decomposition of the rotational levels is the second-order fourth-rank tensor centrifugal distortion T_{044}. Its constant t_{044} was not known until our work on hyperfine interactions and has been determined in ref. [12] from the structures of five hyperfine-induced crossovers; its value is very small, 5.7 Hz, in agreement with theory [39], but its role is essential since it governs the strength of the effects of off-diagonal hyperfine terms.

The operators T_{224} and T_{044} have the following matrix elements in the VR basis:

$$\langle J_\tau M_J RnC v_3 l_3 | T_{224} | J_\tau M_J RnC v_3 l_3 \rangle = \delta_{v_3 1} \langle JRnC | T_{224} | JRnC \rangle , \tag{7}$$

with

$$\langle RRnC | T_{224} | RRnC \rangle = (\tfrac{12}{7})^{1/2} \frac{[(2R-3)\ldots(2R+5)]^{1/2}}{2R(2R+2)} (-1)^R F^4_{A_1\, nC\, nC}{}^{R\ R} ,$$

$$\langle (R+1)RnC | T_{224} | (R+1)RnC \rangle = -\tfrac{1}{2} (\tfrac{12}{7})^{1/2} \frac{[(2R-3)\ldots(2R+5)]^{1/2}}{(2R+2)(2R+3)} (-1)^R F^4_{A_1\, nC\, nC}{}^{R\ R} ,$$

$$\langle (R-1)RnC | T_{224} | (R-1)RnC \rangle = -\tfrac{1}{2} (\tfrac{12}{7})^{1/2} \frac{[(2R-3)\ldots(2R+5)]^{1/2}}{2R(2R-1)} (-1)^R F^4_{A_1\, nC\, nC}{}^{R\ R} ,$$

$$\langle v_3 = 0\, JRnC | T_{044} | v_3 = 0\, JRnC \rangle = \tfrac{1}{2} (\tfrac{12}{7})^{1/2} [(2J-3)\ldots(2J+5)]^{1/2} (-1)^J F^4_{A_1\, nC\, nC}{}^{R\ R} ,$$

$$\langle v_3 = 1\, RRnC | T_{044} | v_3 = 1\, RRnC \rangle = (\tfrac{12}{7})^{1/2} [R(R+1) - 10] \frac{[(2R-3)\ldots(2R+5)]^{1/2}}{2R(2R+2)} (-1)^R F^4_{A_1\, nC\, nC}{}^{R\ R} ,$$

$$\langle v_3 = 1\ (R+1)RnC | T_{044} | v_3 = 1\ (R+1)RnC \rangle$$

$$= (\tfrac{12}{7})^{1/2} [(R+1)^2 + \tfrac{9}{2}(R+1) + 5] \frac{[(2R-3)\ldots(2R+5)]^{1/2}}{(2R+2)(2R+3)} (-1)^R F^4_{A_1\, nC\, nC}{}^{R\ R} ,$$

$$\langle v_3 = 1\ (R-1)RnC | T_{044} | v_3 = 1\ (R-1)RCn \rangle$$

$$= (\tfrac{12}{7})^{1/2} (R^2 - \tfrac{9}{2}R + 5) \frac{[(2R-3)\ldots(2R+5)]^{1/2}}{2R(2R-1)} (-1)^R F^4_{A_1\, nC\, nC}{}^{R\ R} . \tag{8}$$

Since these operators do not act on nuclear spin wavefunctions and do not lift the M_J degeneracy and since the coupled basis is obtained through an orthogonal transformation, we have the same expressions for the matrix elements in the coupled basis:

$$\langle (JI)FM_F; (RnC_R C_S) A_{2u} v_3 \alpha | T_{224} \text{ or } T_{044} | (J'I')F'M'_F; (R'n'C'_R C'_S) A_{2u} v_3 \alpha' \rangle$$

$$= \delta_{II'} \delta_{JJ'} \delta_{C_R C'_R} \delta_{FF'} \delta_{M_F M'_F} \langle JRnC_R v_3 \alpha | T_{224} \text{ or } T_{044} | J'R'n'C'_R v_3 \alpha' \rangle . \tag{9}$$

The coefficients $F^4_{A_1\, nC\, nC}{}^{R\ R}$ which appear in formulae (7) and (8) have been tabulated by Krohn [33]; their numerical values display the clusterization of levels studied at length by Harter and Patterson [14]. Clusters are particularly tight towards the ends of R manifolds and become tighter as R increases; within these tight clusters, vibration–rotation states will be substantially mixed when coupled by off-diagonal matrix elements of nuclear

hyperfine operators. Since all vibration–rotation states within a cluster have different symmetry species C there is no way that this mixing can occur owing to the vibration–rotation hamiltonian alone.

3.2. The spin–rotation hamiltonian

At the nucleus k, the magnetic field created by the relative motions of the electrons and of the other nuclei can be related to the total vibration–rotation angular momentum $\boldsymbol{J}$ through a tensor C^k and the interaction between the magnetic moment of that nucleus and that magnetic field can be expressed as:

$$W_{SR}^k = -\boldsymbol{\mu}^k \cdot \boldsymbol{B}^k = -g_I \mu_N \boldsymbol{I}^k \cdot \boldsymbol{B}^k = -h\boldsymbol{I}^k \cdot C^k \boldsymbol{J}\,, \tag{10}$$

where the components of the nuclear spin $\boldsymbol{I}^k$ and of $\boldsymbol{J}$ as well as C^k are expressed in the space-fixed frame (SFF).

Following what Ozier et al. [34] did for T_d molecules, we can easily derive the expression for C^k in the molecule-fixed frame (MFF). For obvious symmetry reasons, the magnetic field created by J_z (respectively J_x or J_y) will be directed along the z (respectively x or y) axis. In addition, for a nucleus e.g. on the z axis, J_x and J_y will create identical effects; for nuclei 1 and 6 we can write:

$$C^1(\mathrm{MFF}) = C^6(\mathrm{MFF}) = \begin{pmatrix} C_\perp & 0 & 0 \\ 0 & C_\perp & 0 \\ 0 & 0 & C_\parallel \end{pmatrix}. \tag{11}$$

Similarly, for the other nuclei, we have:

$$C^2(\mathrm{MFF}) = C^4(\mathrm{MFF}) = \begin{pmatrix} C_\perp & 0 & 0 \\ 0 & C_\parallel & 0 \\ 0 & 0 & C_\perp \end{pmatrix}, \quad C^3(\mathrm{MFF}) = C^5(\mathrm{MFF}) = \begin{pmatrix} C_\parallel & 0 & 0 \\ 0 & C_\perp & 0 \\ 0 & 0 & C_\perp \end{pmatrix}. \tag{12}$$

Each of these tensors can be written in the form

$$C^k(\mathrm{MFF}) = c_a I + \tfrac{1}{3} c_d \epsilon^k(\mathrm{MFF})\,, \tag{13}$$

where c_a and c_d are called respectively the scalar and the tensor spin–rotation constants†; I is the identity tensor and the $\epsilon^k(\mathrm{MFF})$ are given by:

$$\epsilon^1(\mathrm{MFF}) = \epsilon^6(\mathrm{MFF}) = \begin{pmatrix} 1 & 0 & 0 \\ 0 & 1 & 0 \\ 0 & 0 & -2 \end{pmatrix}, \quad \epsilon^2(\mathrm{MFF}) = \epsilon^4(\mathrm{MFF}) = \begin{pmatrix} 1 & 0 & 0 \\ 0 & -2 & 0 \\ 0 & 0 & 1 \end{pmatrix},$$

$$\epsilon^3(\mathrm{MFF}) = \epsilon^5(\mathrm{MFF}) = \begin{pmatrix} -2 & 0 & 0 \\ 0 & 1 & 0 \\ 0 & 0 & 1 \end{pmatrix}. \tag{14}$$

These $\epsilon^k(\mathrm{MFF})$ satisfy the usual properties: they are symmetric, traceless and therefore transform under rotations according to the $J = 2$ representation; moreover their sum is zero.

The scalar part of $C^k(\mathrm{MFF})$ is of course invariant in the transformation from MFF to SFF and gives rise to the scalar spin–rotation interaction

† With this definition of c_d, one must take $|c_d| = 4.25$ kHz; the value given in ref. [12] is twice c_d.

$$W_{SR}^{S} = -hc_a \sum_k \boldsymbol{I}^k \cdot \boldsymbol{J} . \tag{15}$$

To obtain SFF components of the tensorial part of C^k, ϵ^k, we first derive spherical components $\epsilon_\mu^{(2)k}(\mathrm{MFF})(\mu = 0, \pm 1, \pm 2)$ from the MFF cartesian components $\epsilon_{\alpha\beta}^{k}(\mathrm{MFF})(\alpha,\beta = x, y, z)$ given in (14); Cook and de Lucia [35] have given the relationship between the two sets of components in the general case of a rank-two tensor $T^{(2)}$:

$$T_0^{(2)} = 6^{-1/2}[3T_{zz} - (T_{xx} + T_{yy} + T_{zz})] , \quad T_{\pm 1}^{(2)} = \mp \tfrac{1}{2}[T_{xz} + T_{zx} \pm i(T_{yz} + T_{zy})],$$

$$T_{\pm 2}^{(2)} = \tfrac{1}{2}[T_{xx} - T_{yy} \pm i(T_{xy} + T_{yx})] . \tag{16}$$

In our case this reduces to

$$\epsilon_0^{(2)k} = \sqrt{3/2}\,\epsilon_{zz} ; \quad \epsilon_{\pm 1}^{(2)k} = 0 , \quad \epsilon_{\pm 2}^{(2)k} = \tfrac{1}{2}(\epsilon_{xx}^{k} - \epsilon_{yy}^{k}) \tag{17}$$

and the only non-zero components are

$$\epsilon_0^{(2)k}(\mathrm{MFF}) = -\sqrt{6} \quad (k = 1 \text{ and } 6) ,$$

$$\epsilon_0^{(2)k}(\mathrm{MFF}) = \sqrt{3/2} , \quad \epsilon_{\pm 2}^{(2)k}(\mathrm{MFF}) = \tfrac{3}{2} \quad (k = 2 \text{ and } 4) ,$$

$$\epsilon_0^{(2)k}(\mathrm{MFF}) = \sqrt{3/2} , \quad \epsilon_{\pm 2}^{(2)k}(\mathrm{MFF}) = -\tfrac{3}{2} \quad (k = 3 \text{ and } 5) . \tag{18}$$

The SFF components can now be obtained through the rotation matrices

$$\epsilon_\mu^{(2)k}(\mathrm{SFF}) = \sum_{\mu'} \mathcal{D}_{\mu'\mu}^{(2)}(-\omega)\,\epsilon_{\mu'}^{(2)k}(\mathrm{MFF}) , \tag{19}$$

where we take the inverse rotation $-\omega$ since we use the active representation. We shall couple the rank-two tensors $\epsilon^{(2)k}(\mathrm{SFF})$ with the rank-one tensor $J^{(1)}$ to transform the tensor spin–rotation interaction from

$$W_{SR}^{T} = -\tfrac{1}{3} hc_d \sum_k \boldsymbol{I}^k \epsilon^k(\mathrm{SFF}) \boldsymbol{J} \tag{20}$$

to

$$W_{SR}^{T} = \tfrac{1}{3}\sqrt{5/3}\, hc_d \sum_k I^{(1)k} \cdot [\epsilon^{(2)k}(\mathrm{SFF}) \times J^{(1)}]^{(1)} , \tag{21}$$

where the factor $-\sqrt{5/3}$ accounts for the change of normalisation of the tensor ϵ^k and is given in the appendix of ref. [35].

Now we want to take advantage of the point group symmetry and use irreducible tensors in $^{L}O(3) \times G$ and not in $^{L}O(3)$ only. We shall therefore use the orthogonal matrix $\langle C\sigma|k\rangle$ which relates quantities labeled with one nucleus index k to irreducible O_h tensors:

$$\epsilon_\mu^{(2)k}(\mathrm{SFF}) = \sum_{C,\sigma} \langle C, \sigma|k\rangle \epsilon_{\mu\sigma}^{(2,C)}(\mathrm{SFF}) . \tag{22}$$

As pointed out by Itano [16], the matrix elements $\langle C\sigma|k\rangle$ are identical to the coefficients of the symmetry-adapted nuclear spin wavefunctions with one nuclear spin opposite to the five others, that is to say with $M_I = \pm 2$ (table 1). In the MFF frame, the matrix $\langle C, \sigma|k\rangle$ enables one to define quantities $[\epsilon_\sigma^{(C)}]_\mu^{(2)}(\mathrm{MFF})$:

$$[\epsilon_\sigma^{(C)}]_\mu^{(2)}(\mathrm{MFF}) = \sum_k \langle C, \sigma|k\rangle \epsilon_\mu^{(2)k}(\mathrm{MFF}) , \tag{23}$$

Table 1

$\langle C\sigma\|i\rangle$	1	2	3	4	5	6
A_{1g}	$1/\sqrt{6}$	$1/\sqrt{6}$	$1/\sqrt{6}$	$1/\sqrt{6}$	$1/\sqrt{6}$	$1/\sqrt{6}$
$E_g\,1$	$1/\sqrt{3}$	$-1/2\sqrt{3}$	$-1/2\sqrt{3}$	$-1/2\sqrt{3}$	$-1/2\sqrt{3}$	$1/\sqrt{3}$
$E_g\,2$	0	$-1/2$	$1/2$	$-1/2$	$1/2$	0
$F_{1u}\,x$	0	0	$1/\sqrt{2}$	0	$-1/\sqrt{2}$	0
$F_{1u}\,y$	0	$-1/\sqrt{2}$	0	$1/\sqrt{2}$	0	0
$F_{1u}\,z$	$1/\sqrt{2}$	0	0	0	0	$-1/\sqrt{2}$

for which we can deduce from (18) and table 1 that the only non-vanishing components are

$$[\epsilon_1^{(E_g)}]_0^{(2)}(\mathrm{MFF}) = -3\sqrt{2}\,, \quad [\epsilon_2^{(E_g)}]_{\pm 2}^{(2)}(\mathrm{MFF}) = -3\,. \tag{24}$$

From (22), (19) and (23), we can check that $[\epsilon_\sigma^{(C)}]_\mu^{(2)}(\mathrm{MFF})$ and $\epsilon_{\mu\sigma}^{(2,C)}(\mathrm{SFF})$ are related by rotation matrices [similarly to (19)]:

$$\epsilon_{\mu\sigma}^{(2,C)}(\mathrm{SFF}) = \sum_{\mu'} \mathcal{D}_{\mu'\mu}^{(2)}(-\omega)\,[\epsilon_\sigma^{(C)}]_{\mu'}^{(2)}(\mathrm{MFF})\,.$$

In order to be consistent with ref. [17], we shall use the same O_h symmetry-adapted nuclear spin operators $I_{\mu\sigma}^{(1,C)}$ which turn out to be defined as

$$I_\mu^{(1,A_{1g})} = \sum_k \langle A_{1g}|k\rangle I_\mu^{(1)k}\,, \quad I_{\mu\sigma}^{(1,E_g)} = -2\sum_k \langle E_g\sigma|k\rangle I_\mu^{(1)k}\,, \quad I_{\mu,\sigma}^{(1,F_{1u})} = \sqrt{2}\sum_k \langle F_{1u}\sigma|k\rangle I_\mu^{(1)k}\,. \tag{25}$$

If we substitute these expressions in (15) and (21) and if we recall that the matrix $\langle C\sigma|k\rangle$ is orthogonal, we get:

$$W_{SR}^{S} = -hc_a I^{(1,A_{1g})}\cdot J^{(1,A_{1g})}\,, \tag{26}$$

$$W_{SR}^{T} = \tfrac{1}{3}\sqrt{5/3}\,hc_d(-\tfrac{1}{2})\,I^{(1,E_g)}\cdot[\epsilon^{(2,E_g)}(\mathrm{SFF})\times J^{(1,A_{1g})}]^{(1,E_g)}\,, \tag{27}$$

which we shall write

$$W_{SR}^{T} = \tfrac{1}{3}\sqrt{5/2}\,hc_d[I^{(1,E_g)}\times[\epsilon^{(2,E_g)}(\mathrm{SFF})\times J^{(1,A_{1g})}]^{(1,E_g)}]^{(0,A_{1g})}\,. \tag{28}$$

A key point in the calculation is now to realize that the components of $[\epsilon^{(C)}]^{(2)}(\mathrm{MFF})$ are proportional to the matrix elements of ${}^{(2)}G_\mu^{E_g\sigma}$ which transforms a rank-two spherical basis to a cubic basis [24]; so that we can write

$$\begin{aligned}
[\epsilon^{(2,E_g)}(\mathrm{SFF})\times J^{(1,A_{1g})}]_{\mu\sigma}^{(1,E_g)} &= (-1)^{\mu+1}\sqrt{3}\sum_{\mu_1\mu_2}\begin{pmatrix}2 & 1 & 1\\ \mu_1 & \mu_2 & -\mu\end{pmatrix}\epsilon_{\mu_1\sigma}^{(2,E_g)}(\mathrm{SFF})\,J_{\mu_2}^{(1,A_{1g})}\\
&= \sum_{\mu'}\sum_{\mu_1\mu_2}(-1)^{\mu+1}\sqrt{3}\begin{pmatrix}2 & 1 & 1\\ \mu_1 & \mu_2 & -\mu\end{pmatrix}[\epsilon_\sigma^{(E_g)}]_{\mu'}^{(2)}(\mathrm{MFF})\,\mathcal{D}_{\mu'\mu_1}^{(2)}(-\omega)\,J_{\mu_2}^{(1,A_{1g})}\\
&= \sqrt{1/5}\sum_{\mu'}[\epsilon_\sigma^{(E_g)}]_{\mu'}^{(2)}(\mathrm{MFF})\,[D^{(2,2)}\times J^{(1,0)}]_{\mu\mu'}^{(1,2)} = -3\sqrt{2/5}\sum_{\mu'}{}^{(2)}G_\mu^{E_g\sigma}\,[D^{(2,2)}\times J^{(1,0)}]_{\mu\mu'}^{(1,2)}\\
&= -3\sqrt{2/5}\,[D^{(2,2)}\times J^{(1,0)}]_{\mu\sigma}^{(1,2E_g)}\,,
\end{aligned} \tag{29}$$

and finally we have

$$W_{SR}^{T} = -hc_d\,[I^{(1,E_g)} \times [D^{(2,2)} \times J^{(1,0)}]^{(1,2E_g)}]^{(0,A_{1g})}\,. \tag{30}$$

which is the form of operator suitable to easily calculate the matrix elements according to eq. (4).

One should note the difference with the formula given in ref. [17] where

$$W_{SR}^{T} = \alpha_d\,[[I^{(0,1)} \times D^{(1,1)}]^{(1,2E_g)} \times I^{(1,E_g)}]^{(0,A_{1g})}\,. \tag{31}$$

The two expressions are equivalent as can be seen from the fact that the two operators $[I^{(0,1)} \times D^{(1,1)}]^{(1,2)}$ and $[D^{(2,2)} \times J^{(1,0)}]^{(1,2)}$ have opposite reduced matrix elements in the $|JJ\rangle$ basis:

$$\langle JJ\|[D^{(2,2)} \times J^{(1,0)}]^{(1,2)}\|J'J'\rangle = -\sqrt{15}(-1)^{J+J'}\begin{Bmatrix} 2 & 1 & 1 \\ J & J' & J \end{Bmatrix}(2J+1)[(2J'+1)J(J+1)]^{1/2}$$

$$= -\langle JJ\|[I^{(0,1)} \times D^{(1,1)}]^{(1,2)}\|J'J'\rangle\,. \tag{32}$$

Hence these two operators also have opposite reduced matrix elements in the $|JR\rangle$ basis and the two expressions of W_{SR}^{T} have identical matrix elements provided one takes $\alpha_d = hc_d$.

3.3. The direct spin–spin hamiltonian

The interaction hamiltonian between two magnetic dipoles $\boldsymbol{\mu}^i$ and $\boldsymbol{\mu}^j$ is given by (an additional $\mu_0/4\pi$ factor should appear in the MKSA system):

$$W_{SS}^{ij} = \boldsymbol{\mu}^i\cdot\boldsymbol{\mu}^j/|r_{ij}|^3 - 3(\boldsymbol{r}_{ij}\cdot\boldsymbol{\mu}^i)(\boldsymbol{r}_{ij}\cdot\boldsymbol{\mu}^j)/|r_{ij}|^5\,, \tag{33}$$

where $\boldsymbol{r}_{ij} = \boldsymbol{r}_i - \boldsymbol{r}_j$. It is well known [25] that this can be written with rank-two irreducible tensors made up from the rank-one tensors μ^i:

$$W_{SS}^{ij} = -(\sqrt{6}/|r_{ij}|^3)\sum_{\mu}(-1)^{\mu}C_{-\mu}^{(2)ij}(\mathrm{SFF})[\mu^i \times \mu^j]_{\mu}^{(2)}\,, \tag{34}$$

where $C_{-\mu}^{(2)ij}(\mathrm{SFF})$ is the value of the renormalized spherical harmonic of Racah for the SFF angles θ_{ij} and ϕ_{ij} associated with the vector $\boldsymbol{r}_{ij}$:

$$C_{\mu}^{(2)ij} = (\tfrac{4}{5}\pi)^{1/2}Y_{\mu}^{(2)}(\theta_{ij}, \phi_{ij})\,. \tag{35}$$

If now we relate the magnetic moment to the nuclear spin through

$$\mu^i = g_I\mu_N I^i\,, \tag{36}$$

and if we consider the molecule as a rigid rotator in its equilibrium configuration for which $|r_{ij}| = R$ for adjacent nuclei and $R\sqrt{2}$ for opposite nuclei, we can introduce the coupling constants d_1 and d_2:

$$d_1 = g_I^2\mu_N^2/hR^3\,, \quad d_2 = d_1/2\sqrt{2}\,. \tag{37}$$

The direct spin–spin interaction hamiltonian W_{SS} is then obtained by summing W_{SS}^{ij} over couples of nuclei; in order to take advantage of the orthogonality of the matrix $\langle C\sigma|ij\rangle$ which we shall use in (42) and (43) below, we split W_{SS} into two parts:

$$W_{SS} = \sum_{i<j}W_{SS}^{ij} = W_{SS}^{1} + W_{SS}^{2}\,, \tag{38}$$

where W_{SS}^{1} is the hamiltonian which would result if all nuclei were separated by the distance R:

$$W_{SS}^{1} = -\sqrt{6}\,hd_1\sum_{i<j}\sum_{\mu}(-1)^{\mu}C_{-\mu}^{(2)ij}(\mathrm{SFF})\,[I^i \times I^j]_{\mu}^{(2)}\,, \tag{39}$$

and W^2_{SS} is the complement to W_{SS}:

$$W^2_{SS} = -\sqrt{6}h(d_2 - d_1) \sum_{16,24,35} \sum_{\mu} (-1)^{\mu} C^{(2)ij}_{-\mu}(\mathrm{SFF})[I^i \times I^j]^{(2)}_{\mu} . \tag{40}$$

W^1_{SS} can be dealt with as we did for W_{SR}; first we transform $C^{(2)}(\mathrm{SFF})$ to its MFF components:

$$C^{(2)ij}_{-\mu}(\mathrm{SFF}) = \sum_{\mu'} \mathcal{D}^{(2)}_{\mu'-\mu} C^{(2)ij}_{\mu'}(\mathrm{MFF}) . \tag{41}$$

These MFF components can be calculated numerically with eq. (35) and the MFF angles θ_{ij} and ϕ_{ij} of the equilibrium configuration. The matrix $\langle C\sigma|ij\rangle$ which transforms quantities labeled by couples of indices ij to quantities labeled by IR of O_h yields the following transformation:

$$[I^i \times I^j]^{(2)}_{\mu} = \sum_{C\sigma} \langle C\sigma|ij\rangle [I \times I]^{(2,C)}_{\mu,\sigma} , \tag{42}$$

$$C^{(2)ij}_{-\mu}(\mathrm{MFF}) = \sum_{C\sigma} \langle C\sigma|ij\rangle [C^{(C)}_{\sigma}]^{(2)}_{-\mu}(\mathrm{MFF}) . \tag{43}$$

The matrix elements $\langle C\sigma|ij\rangle$ are identical to the coefficients of nuclear spin wavefunctions with two nuclear spins opposite to the four others, i.e. with $M_I = \pm 1$; they are given in table 2. Because $\langle C\sigma|ij\rangle$ is an orthogonal matrix we can readily write:

$$W^1_{SS} = -\sqrt{6}\hbar d_1 \sqrt{1/5} \sum_{C,\sigma} \sum_{\mu',\mu} (-1)^{\mu} [C^{(C)}_{\sigma}]^{(2)}_{\mu'}(\mathrm{MFF}) D^{(2,2)}_{-\mu\mu'} [I \times I]^{(2,C)}_{\mu\sigma} . \tag{44}$$

Here again we can notice that the numerical values of the $[C^{(C)}_{\sigma}]^{(2)}_{\mu}$ which are derived from (35), (42) and table 2 are proportional to the matrix elements ${}^{(2)}G^{C,\sigma}_{\mu}$ which transform a spherical basis to a cubic basis (see table 3):

$$[C^{(C)}_{\sigma}]^{(2)}_{\mu}(\mathrm{MFF}) = \sqrt{3}\, {}^{(2)}G^{C,\sigma}_{\mu} . \tag{45}$$

If we now express the double dot product of (44) in terms of tensor couplings, we obtain

$$W^1_{SS} = -\hbar d_1 \, 3\sqrt{2}\sqrt{2}[D^{(2,2E_g)} \times [I \times I]^{(2,E_g)}]^{(0,A_{1g})} - \hbar d_1 \, 3\sqrt{2}\sqrt{3}[D^{(2,2F_2)} \times [I \times I]^{(2,F_2)}]^{(0,A_{1g})} . \tag{46}$$

We shall now deal with W^2_{SS}: it can be checked straightforwardly that, with the values of $C^{(2)ij}_{\mu}(\mathrm{MFF})$ calcu-

Table 2

$\langle C\sigma\|ij\rangle$	12	13	14	15	16	23	24	25	26	34	35	36	45	46	56
E_g 1	$\frac{1}{4\sqrt{3}}$	$\frac{1}{4\sqrt{3}}$	$\frac{1}{4\sqrt{3}}$	$\frac{1}{4\sqrt{3}}$	$\frac{1}{\sqrt{3}}$	$\frac{1}{-2\sqrt{3}}$	$\frac{1}{-2\sqrt{3}}$	$\frac{1}{-2\sqrt{3}}$	$\frac{1}{4\sqrt{3}}$	$\frac{1}{-2\sqrt{3}}$	$\frac{1}{-2\sqrt{3}}$	$\frac{1}{4\sqrt{3}}$	$\frac{1}{-2\sqrt{3}}$	$\frac{1}{4\sqrt{3}}$	$\frac{1}{4\sqrt{3}}$
E_g 2	−1/4	1/4	−1/4	1/4	0	0	−1/2	0	−1/4	0	1/2	1/4	0	−1/4	1/4
E'_g 1	$\frac{1}{4\sqrt{3}}$	$\frac{1}{4\sqrt{3}}$	$\frac{1}{4\sqrt{3}}$	$\frac{1}{4\sqrt{3}}$	$\frac{1}{-\sqrt{3}}$	$\frac{1}{-2\sqrt{3}}$	$\frac{1}{2\sqrt{3}}$	$\frac{1}{-2\sqrt{3}}$	$\frac{1}{4\sqrt{3}}$	$\frac{1}{-2\sqrt{3}}$	$\frac{1}{2\sqrt{3}}$	$\frac{1}{4\sqrt{3}}$	$\frac{1}{-2\sqrt{3}}$	$\frac{1}{4\sqrt{3}}$	$\frac{1}{4\sqrt{3}}$
E'_g 2	−1/4	1/4	−1/4	1/4	0	0	1/2	0	−1/2	0	−1/2	1/4	0	−1/4	1/4
F_{2g} x	1/2	0	−1/2	0	0	0	0	0	−1/2	0	0	0	0	1/2	0
F_{2g} y	0	−1/2	0	1/2	0	0	0	0	0	0	0	1/2	0	0	−1/2
F_{2g} z	0	0	0	0	0	1/2	0	−1/2	0	−1/2	0	0	1/2	0	0

Table 3
Values of $[C_\sigma^{(C)}]_\mu^{(2)}$(MFF)

μ	$C\sigma$				
	$F_{2g}x$	$F_{2g}y$	$F_{2g}z$	E_g1	E_g2
± 2	0	0	$\pm i\sqrt{3/2}$	0	$\sqrt{3/2}$
± 1	$-i\sqrt{3/2}$	$\mp i\sqrt{3/2}$	0	0	0
0	0	0	0	$\sqrt{3}$	0

lated by eq. (35), the values $[C^{(E_g)}]^{(2)}$(MFF) given in table 3 and the expressions of $[I^i \times I^j]_\mu^{(2)}$ (obtained by eq. (43) and table 2), we can write the following relation:

$$C_{-\mu}^{(2)16}(\mathrm{MFF})\,[I^1 \times I^6]_\mu^{(2)} + C_{-\mu}^{(2)24}(\mathrm{MFF})\,[I^2 \times I^4]_\mu^{(2)} + C_{-\mu}^{(2)35}(\mathrm{MFF})\,[I^3 \times I^5]_\mu^{(2)}$$

$$= \tfrac{1}{2}\, C_{-\mu}^{(2,E_g)}(\mathrm{MFF})\,\{[I \times I]_\mu^{(2,E_g)} - [I \times I]_\mu^{(2,E_g')}\}\,, \tag{47}$$

whence we can deduce, with the same steps as for W_{SS}^1 that:

$$W_{SS}^2 = -\sqrt{6}h(d_2 - d_1)(\sqrt{3}/2)\sqrt{2}\,[D^{(2,2E_g)} \times \{[I \times I]^{(2,E_g)} - [I \times I]^{(2,E_g')}\}]^{(0,A_{1g})}\,. \tag{48}$$

Finally (46) and (48) can be gathered in the final expression of W_{SS}:

$$W_{SS} = -3h\,[D^{(2,2E_g)} \times \{(d_1 + d_2)[I \times I]^{(2,E_g)} + (d_1 - d_2)[I \times I]^{(2,E_g')}\}]^{(0,A_{1g})}$$

$$-3\sqrt{6}hd_1\,[D^{(2,2F_{2g})} \times [I \times I]^{(2,F_{2g})}]^{(0,A_{1g})}\,, \tag{49}$$

which is in suitable form to calculate the matrix elements. Actually, instead of the operator $[I \times I]_\mu^{(2,C)}$ defined in (42) one can use the operator $S^{(2,C)}$ defined in eq. (44) of ref. [17]. Both sets of operators can easily be expressed in terms of $[I^i \times I^j]_\mu^{(2)}$, which will yield the relationships between our constants d_1 and d_2 and the constants d_1^E, d_2^E, d_3^E and d^F of ref. [17]. In particular we have:

$$S^{(2,F_{2g})} = 2\sqrt{2}\,[I \times I]^{(2,F_{2g})} \tag{50}$$

which leads to

$$d_F = -\tfrac{3}{2}\sqrt{3}hd_1\,. \tag{51}$$

If we consider then the combination

$$d_{1_{A_{1g}}}^E S^{(2,E_g)} + d_{2_{E_gE_g}}^E S^{(2,E_g)} + d_{3_{F_{1u}F_{1u}}}^E S^{(2,E_g)}\,,$$

in terms of $[I^i \times I^j]_\mu^{(2)}$, and try to identify it to

$$(d_1 + d_2)[I \times I]^{(2,E_g)} + (d_1 - d_2)[I \times I]^{(2,E_g')}\,,$$

we must (i) cancel the coefficients of $[I^i \times I^i]_\mu^{(2)}$, (ii) identify the coefficients of $[I^i \times I^j]_\mu^{(2)}$ with $(ij) \neq (16), (24)$ or (35), (iii) identify the coefficients of $[I^i \times I^j]_\mu^{(2)}$ with $(ij) = (16), (24)$ or (35); this respectively leads to the three equations:

$$3d_1^E + \sqrt{6}d_2^E + (3/\sqrt{2})d_3^E = 0 \quad \text{(coefficient of } I^iI^i)\,,$$

$$-d_1^E/\sqrt{3} + \tfrac{2}{3}\sqrt{2}d_2^E = -(3/4\sqrt{3})h[d_1 + d_2 + (d_1 - d_2)] = -(\sqrt{3}/2)hd_1 \quad \text{(coefficient of } I^1I^2\text{)},$$

$$-(8/\sqrt{3})d_1^E - \tfrac{8}{3}\sqrt{2}\,d_2^E = -(3/4\sqrt{3})4h[d_1 + d_2 - (d_1 - d_2)] = -2\sqrt{3}hd_2 \quad \text{(coefficient of } I^1I^6\text{)}, \quad (52)$$

from which we deduce the relationships between the two sets of constants:

$$d_2^E = \tfrac{1}{2}\sqrt{3/2}\,h(\tfrac{1}{2}d_2 - d_1), \quad d_1^E = \tfrac{1}{2}h(d_2 + d_1), \quad d_3^E = -(3/2\sqrt{2})hd_2. \quad (53)$$

3.4. The spin–vibration interaction

In our previous work [2,9] on the hyperfine structures of three A_2 VR lines (R 28 A_2^0, P 33 A_2^1 and P 59 A_2^3), we have been obliged to introduce the scalar spin–vibration hamiltonian which can simply be written as:

$$W_{SV}^S = hA\boldsymbol{I}\cdot\boldsymbol{l}_3, \quad (54)$$

where $\boldsymbol{l}_3$ is the vibrational angular momentum associated with the triply degenerate mode ν_3 we are concerned with, $\boldsymbol{I}$ is the total nuclear spin, $\boldsymbol{I} = \Sigma_{1,6}\boldsymbol{I}^i$, and where both vectors have to be considered in the same frame. As pointed out in ref. [36], if R is considered as a good quantum number, the diagonal matrix elements can be derived by the vector model ($\langle \boldsymbol{I}\cdot\boldsymbol{l}\rangle = \langle \boldsymbol{I}\cdot\boldsymbol{J}\rangle\langle \boldsymbol{J}\cdot\boldsymbol{l}\rangle/\langle J^2\rangle$) which leads to:

$$\langle J_\tau R_{\tau\times u} nC_{VR}; IC_S, \nu_3 = 1 | W_{SV}^S | J_\tau R_{\tau\times u} nC_{VR}; IC_S, \nu_3 = 1\rangle$$

$$= -[Ah/4J(J+1)][F(F+1) - J(J+1) - I(I+1)][R(R+1) - J(J+1) - 2]. \quad (55)$$

In this formula, one can see that the effect of this operator is much larger in P and R branches than in the Q branch, where $R = J$ in the $\nu_3 = 1$ level. The same matrix elements would be obtained with the formalism developed in sections 3.2 and 3.3; if SFF components of I are used in (54), we can write

$$W_{SV}^S = -hA\sqrt{3}[I^{(1,A_{1g})} \times [D^{(1,1)} \times l_3^{(0,1)}]^{(1,0A_{1g})}]^{(0,A_{1g})}, \quad (56)$$

in agreement with the operator given by Michelot [30].

The treatment of the interaction between nuclear spins and the magnetic field created by the angular momentum $\boldsymbol{J}$ can be repeated for the magnetic field created by the vibrational angular momentum $\boldsymbol{l}_3$. Therefore we obtain similar interaction operators: indeed (56) is analogous to (26) and there exists also a tensor spin–vibration interaction [30], analogous to (31) (and derived by Uehara et al. [36] for T_d molecules):

$$W_{SV}^T = X[I^{(1,E_g)} \times [D^{(1,1)} \times l_3^{(0,1)}]^{(1,2E_g)}]^{(0,A_{1g})}, \quad (57)$$

where the constant X is unknown up to now. For a given value of J and R in the $\nu_3 = 1$ state, this operator has matrix elements which are proportional to those of W_{SR}^T so that we can introduce W_{SV}^T phenomenologically by varying c_d in the $\nu_3 = 1$ level (we proceeded in the same way to determine A). Once we have several Δc_d for different vibration–rotation clusters, then we can show that all these effective Δc_d stem from a unique spin–vibration coupling constant X. For the time being we have only varied c_d in the excited vibrational state for one cluster, P(82) $F_1^{10}F_2^{10}$ [section 4 example (C)], and one line, P(4) F_1 [example (D)]; these variations did improve the theoretical spectra but the values of Δc_d are still tentative and not really adjusted. From the analysis of the great number of well-resolved structures now available we expect to derive in the near future a precise value for the constant X. Also the breakdown of R as a good quantum number might then be manifest in the hyperfine spectrum.

4. Application to the analysis of superfine/hyperfine structures

In this section, we apply the results of section 3 to derive several synthetic spectral structures in the ν_3 band and we compare them with observed spectra. Two such spectra were discussed in ref. [12]; we shall first give more details on these two examples, then we shall display a few other cases for which a comparison between theory and experiment has been performed.

The calculation is made according to the simple following procedure:

(i) In each vibrational state (i.e. the ground state and the $\nu_3 = 1$ state), we consider the vibration–rotation states which are supposedly close enough to interact substantially through hyperfine interactions with the states involved in the observed transitions. It will naturally often be limited to the states belonging to the same cluster but nothing impedes us from considering several adjacent clusters simultaneously or any state belonging to the same J manifold if necessary.

(ii) Each vibration–rotation wavefunction is coupled to nuclear spin wavefunctions in order to construct the total Pauli-allowed wavefunctions which were considered in the previous sections. All these total wavefunctions define the basis of the two subspaces (upper and lower) to which we restrict our calculation. A shorthand notation for these total state vectors will be $|\nu_3 JRC^n_{VR} IF\rangle$ (M_F is ignored in the following); the dimension of each subspace is noted d and is the same for $\nu_3 = 0$ and for $\nu_3 = 1$ because of the selection rules $\Delta R = \Delta C = 0$ (except for $\Delta J = \pm 1$ and if $J < I$ in one of the subspaces, which occurs only if $J \leqslant 3$).

(iii) The hamiltonian matrix is then calculated in each of the subspaces and diagonalized. The matrix is diagonal in the quantum number F and the eigenvector will be noted $|\nu_3 JRFi\rangle$ and can be expressed as

$$|\nu_3 JRFi\rangle = \sum_{CI} \alpha^{(F\nu_3)}_{i,CI} |\nu_3 JRC^n_{VR} IF\rangle .$$

In addition to the block diagonal form in F, non-zero off-diagonal matrix elements appear only if $C_{VR} \times C'_{VR}$ contains the IRs A_{1g}, E_g or F_{2g}, and the eigenvectors are obtained by diagonalizing subblocks of small dimensions (a few units) even if the dimension d can reach a few tens (actually some $|\nu_3 JRC^n_{VR} IF\rangle$ are already eigenvectors).

(iv) The spectrum is deduced from the eigenvalues and eigenvectors; in saturation spectroscopy, to each couple of dipole-allowed transitions which share a common level (either upper or lower) corresponds a line [37]. If the two transitions of the couple are identical, only two levels are involved and the line is located at the frequency of the transition; if the two transitions are different, the line is located half-way between the frequencies of the two transitions and is called a cross-over resonance. The intensities are calculated according to the standard formulae for hyperfine components in saturation spectra [37] in which the individual reduced transition moments are given by

$$\langle \nu_3 JRFi \| \mu \| \nu'_3 J'RF'j \rangle = \sum_{CI} \alpha^{(F,\nu_3)}_{i,CI} \alpha^{(F',\nu'_3)}_{j,CI} \times \langle \nu_3 JRCIF \| \mu \| \nu'_3 J'RCIF' \rangle .$$

The reduced matrix elements in the coupled basis are then related, as usual, (see eq. (17) of ref. [37]) to the reduced element $\langle \nu_3 JRC \| \mu \| \nu'_3 J'RC \rangle$ which can be considered as a constant for each manifold under study.

(v) The synthetic spectrum is then drawn after convolution of the above spectrum with a lineshape function taken as the derivative of a lorentzian whose linewidth (identical for each line) is adjusted for each experiment. If the comparison with the observed spectrum is not satisfactory, the constants of the hamiltonian are changed and we go back to (iii) until agreement is reached; t_{044} and c_d have been determined in this way.

The above procedure of calculation is referred to by Harter [38] as a conventional synthetic approach which yields accurate spectra and constants but does not tell the physical meaning of the eigenvectors. On the other hand, he has developed an analytic approach which enables one to predict what pattern of levels should be expected when the vibration–rotation splittings within a cluster are negligible in comparison with hyperfine matrix elements. This approach relies on the group theory which is generally used for atomic electronic orbitals but which can be applied to molecular nuclear states in the particular case where the rotation axis of the molecule is well stuck to a symmetry axis of the molecule: the symmetry axis is then considered as oriented in the laboratory frame and the nuclear orbitals together with the nuclear spins are used to build a basis of Slater states in which an approximate hyperfine hamiltonian matrix is easy to write down. Harter

[38] has shown that the eigenvectors of this hamiltonian are closely related to symmetry-adapted functions in the groups $S_4 \times S_2$ for tetragonal clusters or $S_3 \times S_3$ for trigonal clusters; this leads to a good physical understanding of the hyperfine splittings: the spin–rotation interaction yields substates which are labeled with broken tableaus (in $S_4 \times S_2$ or $S_3 \times S_3$) and the spin–spin interaction modifies these splittings through a tunneling effect between equivalent states which have the same number of spins up and spins down. However, there are some severe drawbacks in using this method to deduce molecular constants: one introduces a phenomenological hamiltonian for each case (a D_{4h}-invariant hamiltonian for four-fold clusters and a D_{3d}-invariant for three-fold clusters) with a set of effective parameters for each cluster; complications arise as the clusterization becomes weak (frame transformation [43,44] is then required); also the exchange of more than two spins and diagonal spin–spin matrix elements require adding more parameters; altogether to do accurate calculations, it may not be worth pushing the model too far since it starts with an approximate hamiltonian anyway; but it is worth remembering the level classification in the ideal situation and the correlation diagram. We shall try to give the reader the possibility to estimate how the results which come out of hamiltonian matrix and which represent the "real thing" can fit in this model.

To do so we shall give details which will be, for example, the main effects of the respective operators: successive changes in the pattern of levels can be outlined after the introduction of:

(i) the vibration–rotation operators T_{044} and T_{224},
(ii) the scalar spin–rotation operator,
(iii) the diagonal part of the tensor spin–rotation and spin–spin operators,
(iv) the off-diagonal part of these operators.

The strength of the mixing should then be apparent and help the reader to understand the intensities and structures of crossovers. In addition to Q(53) $F_1^6F_2^6$ (example A) and to Q(38) $F_2^0E^0F_1^0$ (example B), we shall show crossovers in the following clusters: Q(54) $A_2^2F_2^7E^4$, Q(41) $F_1^9E^5F_2^8$ and P(82) $F_1^{10}F_2^{10}$ (example C); then we shall show that crossovers also appear to be fairly strong even in a low-J manifold such as P(4) (example D). In P(4) also, a recent spectrum with an improved resolution shows the structure of a main line: the F_1 line splittings are essential to determine the sign of the constant c_d. Finally R(28) A_2^0, shown at the bottom of fig. 1 is another case of resolved hyperfine components and will be our last example (E) to be discussed.

(A) Q(53) $F_1^6F_2^6$

The possible spin wavefunctions are $|F_{2u}, I = 1\rangle$, $|F_{2g}, I = 1\rangle$ for an F_1 vibration–rotation state (which appears to be F_{1g} and F_{1u}), and $|F_{1u}, I = 0\rangle$, $|F_{1u}, I = 2\rangle$ for an F_2 one (which appears to be F_{2g} only). The dimensions of the two matrices built in the basis $|\upsilon_3 JRC_{VR}^n IF\rangle$ are then twelve but each matrix can readily be split into subblocks: the only subblocks with dimension >1 are: one of dimension three spanned by $|\upsilon_3, 53, 53, F_{1g}^6, 1, 53\rangle$, $|\upsilon_3, 53, 53, F_{2g}^6, 0, 53\rangle$ and $|\upsilon_3, 53, 53, F_{2g}^6, 2, 53\rangle$, one of dimension two spanned by $|\upsilon_3, 53, 53, F_{1g}^6, 1, 54\rangle$ and $|\upsilon_3, 53, 53, F_{2g}^6, 2, 54\rangle$ and a last one of dimension two spanned by $|\upsilon_3, 53, 53, F_{1g}^6, 1, 52\rangle$ and $|\upsilon_3, 53, 53, F_{2g}^6, 2, 52\rangle$. The two matrices in $\upsilon_3 = 0$ and $\upsilon_3 = 1$ spaces have exactly the same structure but a very important difference (fig. 3) stems from the fact that the F_1F_2 vibration–rotation splitting due to T_{044} and T_{224} is of the order of 13 MHz for $\upsilon_3 = 1$ and 180 kHz for $\upsilon_3 = 0$. Such a difference appears in all cases and arises because $t_{224} \gg t_{044}$ and because T_{224} has no non-zero matrix elements in the ground state. The influence of off-diagonal matrix elements between F_1 and F_2 will then be almost negligible in the $\upsilon_3 = 1$ state and we shall focus on the ground state.

The scalar spin–rotation interaction alone gives the pattern shown in the second column of fig. 2 which is already very close to Harter's "case two" since it spreads over 1100 kHz. The diagonal part of all the tensor hyperfine operators brings quantitatively small changes (third column) but, qualitatively, the splittings between F_{1g} and F_{1u} subcomponents are an important fact which must be noticed. At this stage and though hyperfine splittings are dominant, there is no point in changing the labeling of states. The result of diagonalization of the three subblocks of interacting states is shown in the right column: in the 2×2 subblocks, the levels are only slightly pushed apart and the two coefficients of each eigenvector are of the order of 0.96 and 0.28 so that they still can be labeled more exactly with the quantum numbers of the original coupled wavefunctions rather than with the broken tableaus which correspond to a $(\sqrt{2}/2, \sqrt{2}/2)$ mixing. On the other hand, in the $(F = 53)$ 3×3 subspace, the

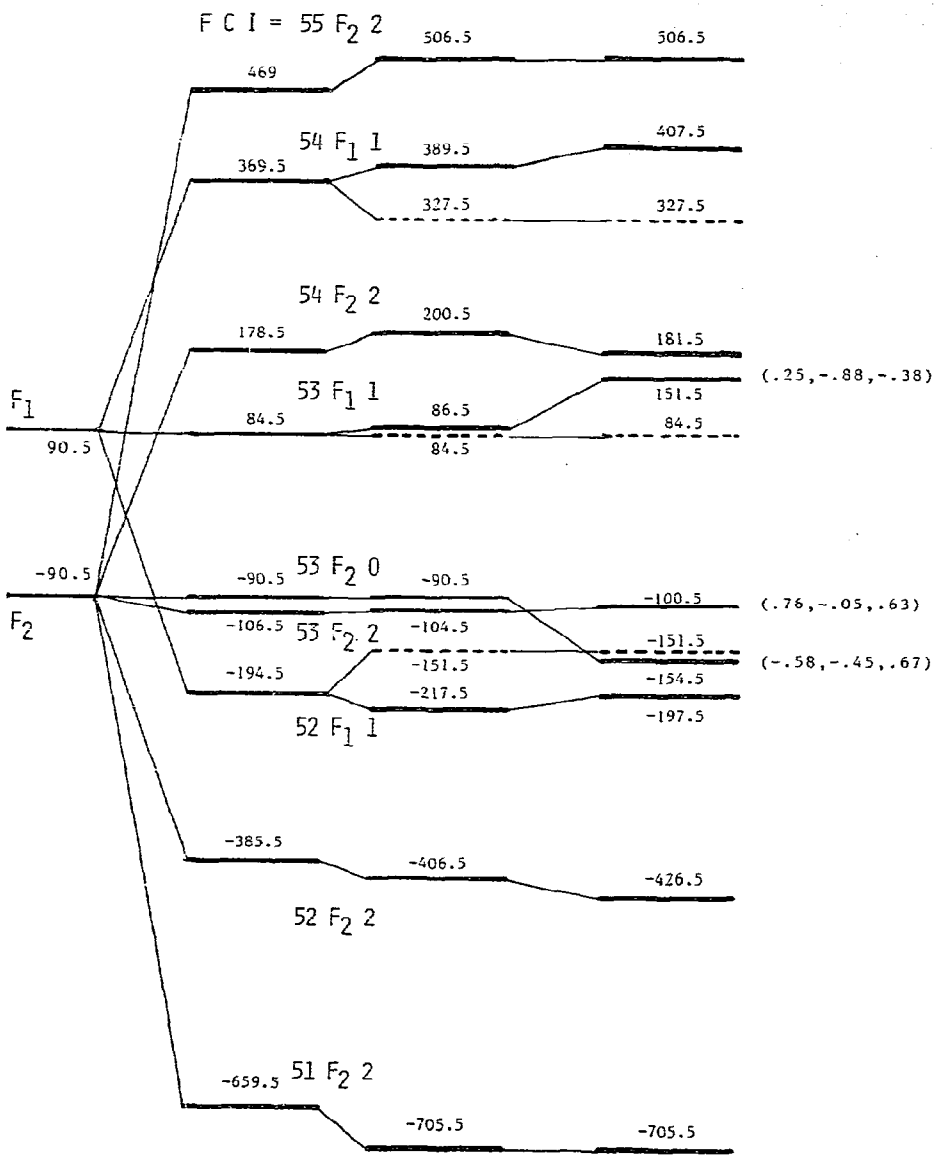

Fig. 2. Q(53) $F_2^6F_1^6$. Patterns of energy levels in the $\nu_3 = 0$ state at successive stages of the calculation; from left to right: VR splitting; scalar spin–rotation splittings; diagonal effects of all hyperfine operators; post-diagonalization pattern. Energies are given in kHz; u states are drawn with dotted lines. For the three ($F = 53$)g levels, we display at the right, in parentheses, the three components of the eigenvectors on the basis ($|F_2 2\rangle$, $|F_1 1\rangle$, $|F_2 0\rangle$).

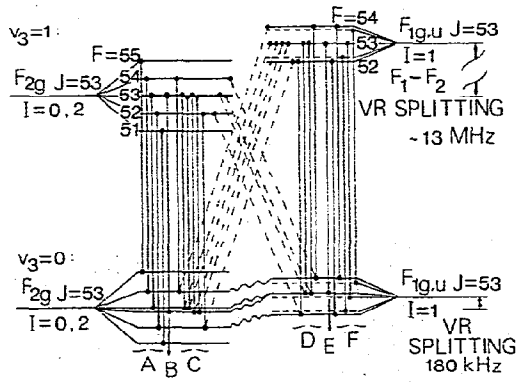

Fig. 3. $Q(53)F_2^6F_1^6$. Energy level diagram for both levels of $Q(53)F_2^6-F_1^6$ and associated resonances. Only main resonances and crossovers of interest for the present discussion are represented.

Table 4

	C,I		
	$F_{1g},2$	$F_{2g},1$	$F_{2g},0$
Scalar	−106.5	–	–
E spin–rotation	−1.16	−73	–
F_2 spin–spin	−0.05	−0.004	−0.07
E spin–spin	3.2	−0.07	−1.2
$F = 53$		84.5	–
		−0.4	103
		−0.2	–
		2.3	–
$\upsilon_3 = 0$			−90.5
			–
			–
			–

mixing is so pronounced that the F_{1g} or F_{2g} character and the value of the total nuclear spin are lost. The components of the eigenvectors (with decreasing eigenvalues) can be compared to those of the broken tableaus which diagonalize the spin–rotation matrix in an exact case 2 (see table VII(c) of ref. [38]): they are respectively (0.25, −0.88, −0.38) versus $(\sqrt{6}/6, -\sqrt{2}/2, -\sqrt{3}/3)$, (0.76, −0.05, 0.63) versus $(\sqrt{6}/3, 0, \sqrt{3}/3)$ and (−0.58, −0.45, 0.67) versus $(\sqrt{6}/6, \sqrt{2}/2, -\sqrt{3}/3)$ and one might be tempted to identify our eigenvectors with the broken tableaus $|^{\uparrow\uparrow\uparrow}_{\downarrow}\downarrow\downarrow\rangle$, $|^{\uparrow\uparrow\downarrow}_{\uparrow}\uparrow\downarrow\rangle$ and $|^{\uparrow\downarrow\downarrow}_{\downarrow}\uparrow\uparrow\rangle$; however the comparison with fig. 17 of ref. [38] ‡ brings the following comments: in our pattern, diagonalization causes a state with $F = 53$ to cross a state with $F = 52$ and this does not appear in Harter's fig. 17; this flaw however is less pronounced in his pattern of fig. 19 after frame transformation.

In order to compare the effects of various terms, we give (table 4) the $3 \times 3 (F = 53)$ matrix in which, for each matrix element, we separate the scalar matrix elements (vibration–rotation + spin–rotation), the E tensor spin–rotation, the F_2 tensor spin–spin and the E tensor spin–spin matrix elements respectively; it can be checked that the spin–spin interaction is only a small perturbation compared to off-diagonal spin–rotation terms.

‡ The values given by Harter for S, τ and a in his caption to fig. 19 and his table XI(c), do not correspond to his fig. 17; one should probably read $a = +0.2$ instead of -0.2.

In the $\upsilon_3 = 1$ state, each vibration–rotation level is split into subcomponents exactly as it is in the third column but, because F_1 and F_2 are separated by 13 MHz, diagonalization has negligible effects. As a consequence, lines involving lower states which are not affected either by diagonalization in fig. 2, will be superposed (e.g. the three F_{1u} $F = 52, 53, 54$ components); on the contrary, if a state is pushed upward (respectively downward) by diagonalization in fig. 2, a transition which involves it will be shifted to the red (respectively blue), e.g. F_{1g} $F = 53$ is pushed upward by 60 kHz and the associated line is 60 kHz left of the F_1 line (see line E in figs. 3 and 5).

(B) $Q(38)F_2^0E^0F_1^0$

The possible spin wavefunctions for an E vibration–rotation state are $|E_g, I = 1\rangle$ and $|E_g, I = 2\rangle$ so that the dimension of the hamiltonian matrix is twenty in each vibrational state; the coupled basis vectors are:

$|\upsilon_3, 38, 38, F_{1g}^0, I = 1, F = 37, 38 \text{ and } 39\rangle$,

$|\upsilon_3, 38, 38, F_{1u}^0, I = 1, F = 37, 38 \text{ and } 39\rangle$,

$|\upsilon_3, 38, 38, E_u^0, I = 1, F = 37, 38 \text{ and } 39\rangle$,

$|\upsilon_3, 38, 38, E_u^0, I = 2, F = 36, 37, 38, 39 \text{ and } 40\rangle$,

$|\upsilon_3, 38, 38, F_{2g}^0, I = 0, F = 38\rangle$,

$|\upsilon_3, 38, 38, F_{2g}^0, I = 2, F = 36, 37, 38, 39 \text{ and } 40\rangle$.

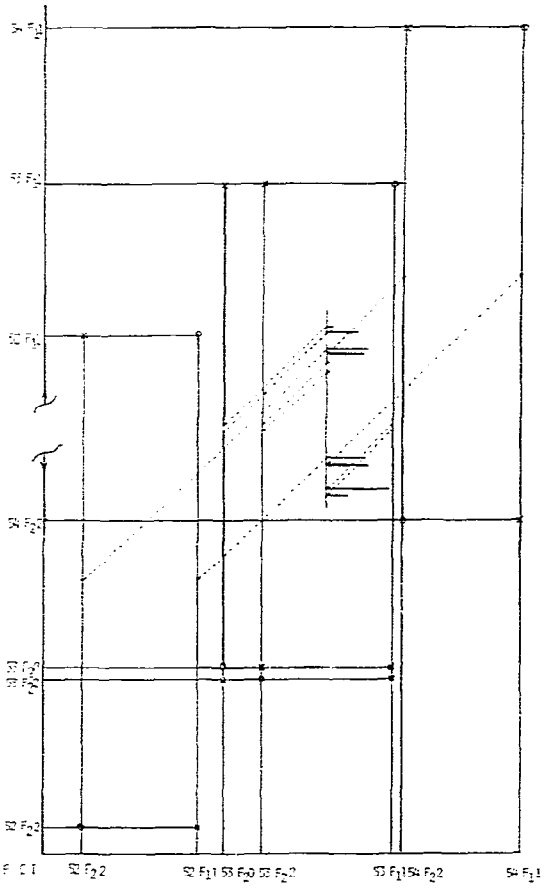

Fig. 4. $Q(53)F_2^6F_1^6$. Nomogram [43] for the crossover lines. Each of the ten crossover lines can be identified and the crossover structure can be related to the patterns of levels in the upper and lower states: the quadruplet is made of two 40 kHz doublets separated by 200 kHz. Two crossover lines have negligible intensities which is explained by the value 0.05 for the F_1 component of the $F_2 2$ eigenvector (see fig. 2).

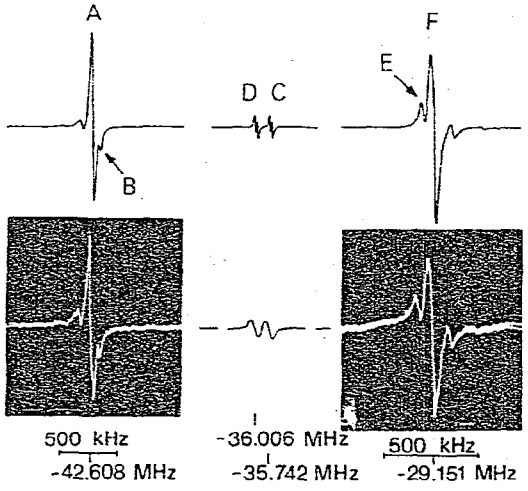

Fig. 5. $Q(53)F_2^6F_1^6$. Calculated (top) and observed (bottom) saturation spectra. This spectrum has been obtained with a free-running laser and the corresponding linewidth is 20 kHz (hwhm). Measured detunings are from $Q(45)F_2^7$.

Since $E_g \times F_{1\tau} = F_{1\tau} + F_{2\tau}$, the tensor spin–rotation interaction can only couple F_{1g}^0 with F_{2g}^0 while, since $F_{2g} \times F_{1\tau} = A_{2\tau} + E_\tau + F_{1\tau} + F_{2\tau}$, the tensor spin–spin interaction can couple E_u^0 with F_{1u}^0 and F_{1g}^0 with F_{2g}^0; if we compare with example (A), we have merely added E_u states which can interact with F_{1u} states through the F_{2g} tensor spin–spin operator only. The coupled states with $F = 36$ or 40 are then already eigenvectors; states with $F = 37$ span two blocks: one of dimension three with E_u and F_{1u} states, the other of dimension two with F_{1g} and F_{2g} states (and similarly for $F = 39$); in the $F = 38$ subspace, we have two blocks of dimension three: one with u states, the other with g states. As in (A), we display the $\nu_3 = 0$ pattern of states at each stage of the calculation and one can see that it

Table 5

	C, I		
	$F_{1u}, 1$	$E_u, 2$	$E_u, 1$
Scalar	204	–	–
E spin–rotation	−0.04	–	–
F_2 spin–spin	4.5	9.8	3.2
E spin–spin	0.0005	–	–
$F = 39$		190	–
		−0.05	+0.2
		–	–
		−0.003	−0.01
$\nu_3 = 0$			200
			−0.05
			–
			+0.007

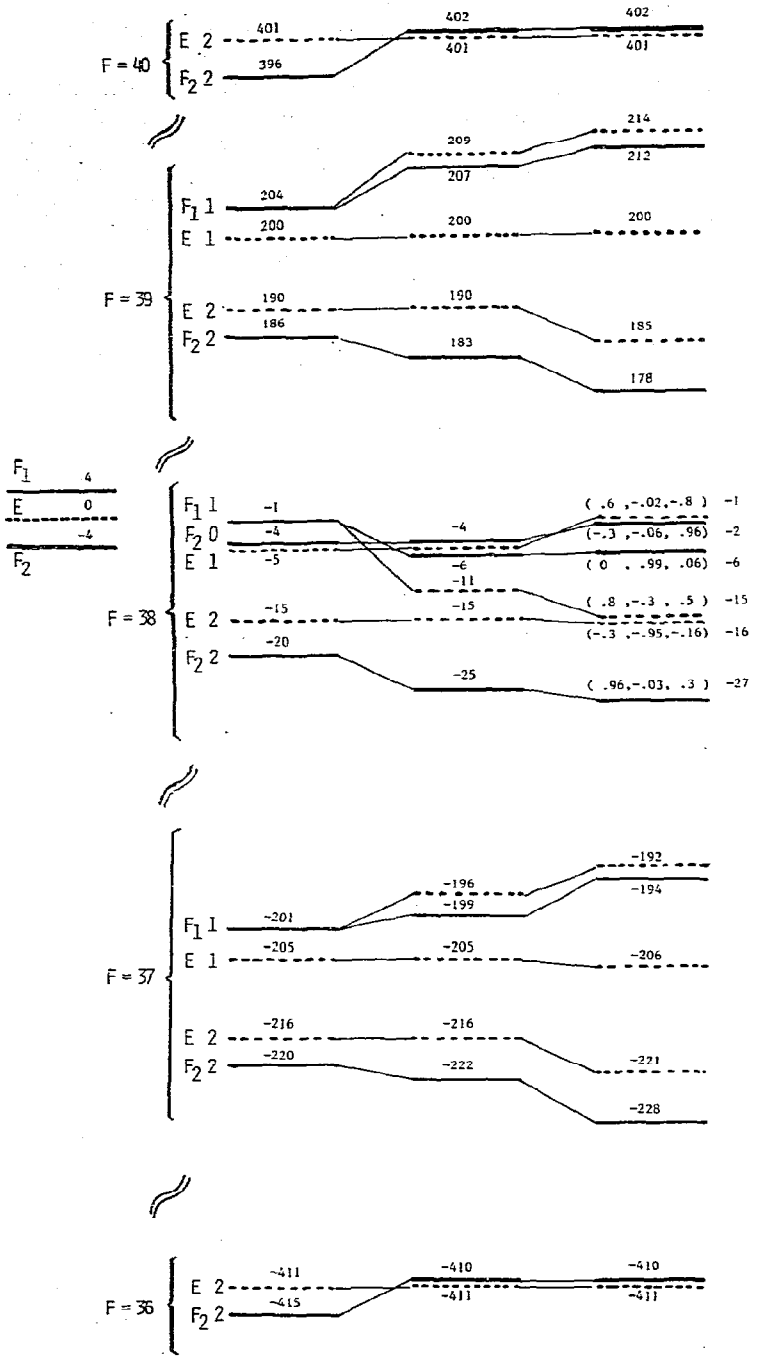

Fig. 6. $Q(38)F_2^0E^0F_1^0$. Patterns of energy levels in the $v_3 = 0$ state at successive stages of the calculations; from left to right: VR splitting; scalar spin–rotation splittings, diagonal effects of all hyperfine operators; post-diagonalization pattern. Energies are given in kHz; u states are drawn with dotted lines. For $F = 38$, the energies after diagonalization are on the right and, on the levels, are displayed the components of the eigenvectors in the basis $(|F_2 2\rangle, |F_1 1\rangle, |F_2 0\rangle)$ for g levels and in the basis $(|F_1 1\rangle, |E1\rangle, |E2\rangle)$ for u levels.

is even much closer to a case 2 than example (A); however, due to the numerical values of the isoscalar coefficients K (see the appendix), the E_g-tensor interactions have much smaller matrix elements and the major mixing stems only from the F_{2g} spin–spin operator whose constant is smaller than c_d; finally the values of the off-diagonal matrix elements are still of the order of the difference between diagonal elements (see the $F = 39$ matrix in table 5); as a consequence, the mixing of basis functions is substantial though the values of the energies are not changed drastically after diagonalization.

The coefficients of the eigenvectors are displayed at the right of fig. 6 and explain the very remarkable crossovers, between E and F_1 lines, shown in fig. 7. The structure and intensities of these crossovers reflect the the fact that, in $F = 39$ or 37 subspaces, the mixing is rather between $|E_u, I = 2\rangle$ and $|F_{1u}, I = 1\rangle$ while in the $F = 38$ subspace, it is rather between $|F_{1u}, I = 1\rangle$ and $|E_u, I = 1\rangle$. One can also note the particular mixing in the $(F = 38)$g matrix where, after diagonalization, F_{1g} stays almost pure while only $|F_{2g}, I = 0\rangle$ and $|F_{2g}, I = 2\rangle$ are really mixed (a comparable mixing between these two states occurs in the $\nu_3 = 1$ level since they are directly coupled by the F_{2g}-tensor spin–spin operator); fortunately F_{1g} and F_{2g} are substantially mixed in the $F = 39$ and $F = 37$ subspaces so that crossovers do occur, as in example (A); however these crossovers are blended with the hyperfine components of the E_u^0 vibration–rotation line.

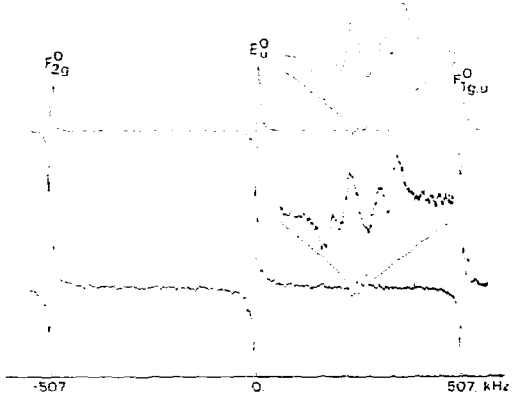

Fig. 7. Calculated (top) and observed (bottom) spectra for the $Q(38)F_2^0E^0F_1^0$ trigonal cluster. This spectrum has been obtained with a frequency offset-locked laser [2] and the linewidth is 5 kHz (hwhm).

(C) More crossovers and superfine structures

In examples (A) and (B), we gave details about two of the crossover structures used in ref. [12] to determine t_{044} and c_d; the other structures we used were in two other $F_1^6F_2^6$ clusters, of Q(51) (which can be seen in fig. 11) and of Q(55), respectively, which are very similar to case A, and another tetragonal cluster, $Q(54)\,A_2^2F_2^7E^4$, which we display in fig. 8. This cluster is simple since F_2VR states are g only and do not interact with A_2 and E which are u only. The crossovers arise because A_2 and E are coupled through the E-tensor spin–rotation interaction only and are thus very sensitive to the value of c_d. In fig. 8, one can see another cluster $Q(41)\,F_1^9E^5F_2^8$ analogous to the Q(38) one of example (B), in which a crossover appears, similarly, between the E^5 and F_1^9 lines. However, the structure of this crossover which is a doublet with 40 kHz splitting is not resolved in the figure.

With the $P(82)\,F_2^{10}F_1^{10}$ cluster shown in fig. 9 we have new interesting features: first the crossover does appear to be a quadruplet, second the main lines F_1 and F_2 exhibit many bumps which were not seen in the previous examples. The theoretical spectrum drawn with the known constants did not reproduce well these bumps of the main lines and we introduced phenomenologically the tensor spin–vibration operator as a correction to the tensor spin–rotation interaction in the $\nu_3 = 1$ state; since these two interactions give the same hyperfine structure this is indeed equivalent to varying c_d in the upper state. The synthetic spectrum

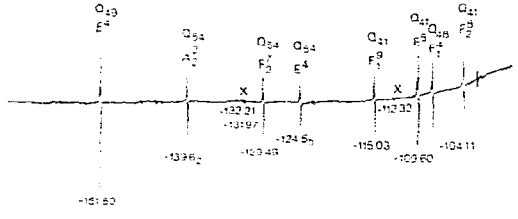

Fig. 8. Portion of the SF_6 saturation spectrum obtained with the P(16) line of the CO_2 waveguide laser [7] illustrating two different cluster patterns: the tetragonal $Q(54)\,A_2^2F_2^7E^4$ cluster with a 2 to 1 superfine splittings ratio and the trigonal $Q(41)\,F_1^9E^5F_2^8$ cluster with almost equal splittings. Crossovers are marked with an X and occur half-way between components of identical parity: the crossover between $Q(54)A_{2u}$ and E_u is clearly resolved as a doublet whereas the structure of the crossover between $Q(41)F_1^9$ and E^5 is unresolved. Frequency detunings are in MHz from the $Q(38)E^6$ line at 28.412 582 469 THz [11].

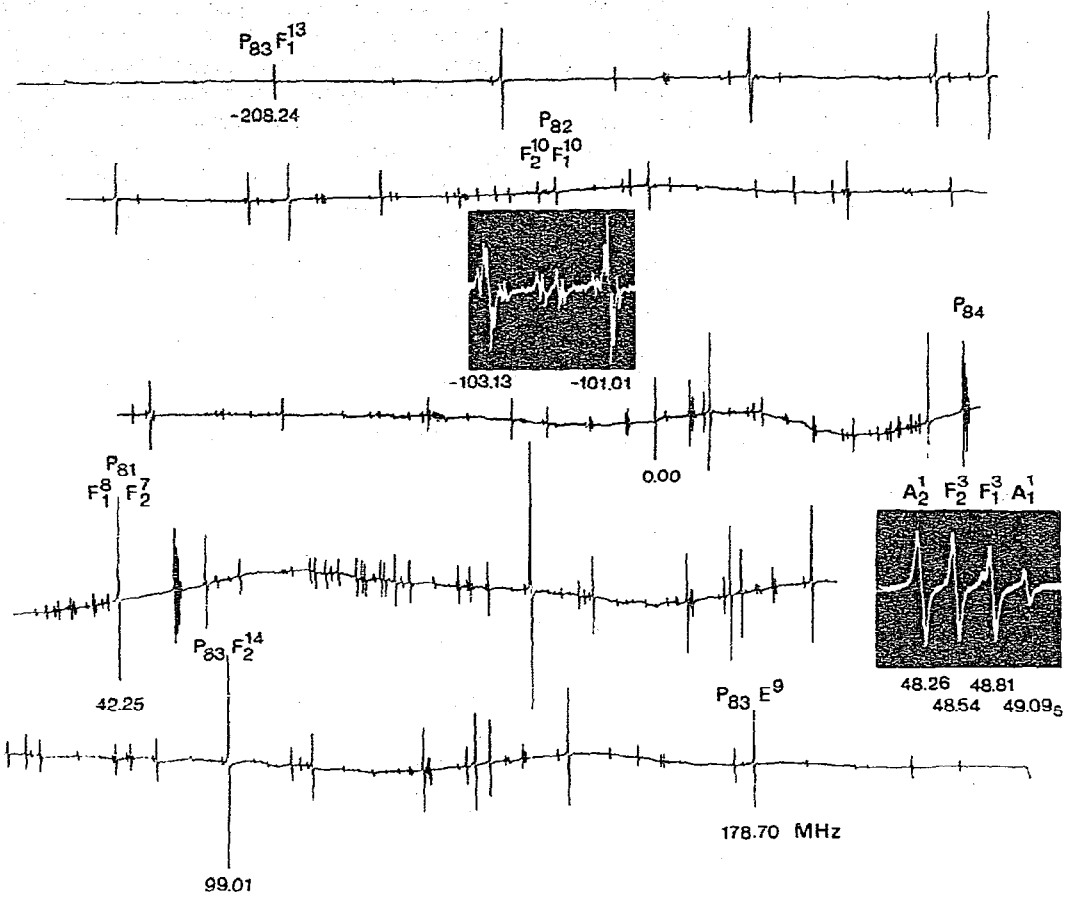

Fig. 9. SF_6 saturation spectrum ranging over 250 MHz on either side of the P(22) CO_2 laser line. Frequency detunings are in MHz from the reference line at 28.251 957 355 THz [11]. Two different cluster patterns are illustrated: the $P(82)F_2^{10}F_1^{10}$ four-fold axis cluster and the $P(84)A_2^1F_2^3F_1^3A_1^1$ three-fold axis cluster with three equal splittings.

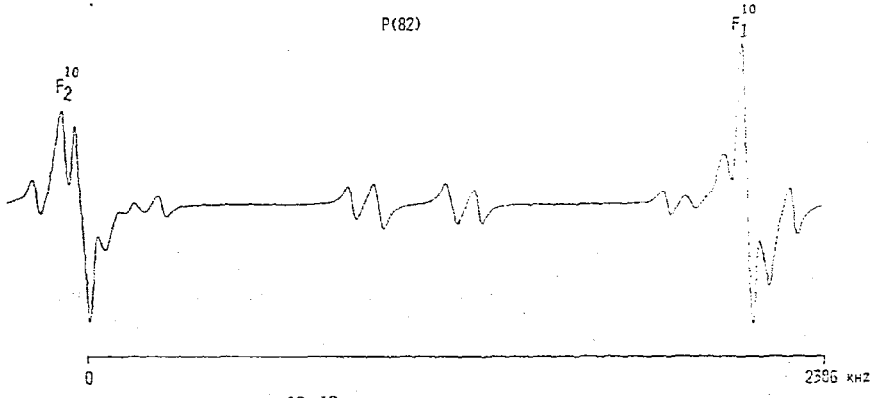

Fig. 10. Synthetic spectrum of $P(82)F_2^{10}F_1^{10}$ cluster drawn with $c_d(\nu_3 = 1) = 1.05\ c_d\ (\nu_3 = 0)$. hwhm = 23.5 kHz.

shown in fig. 10 is drawn with $c_d(v_3 = 0) = 4.25$ kHz and $\Delta c_d = c_d(v_3 = 1) - c_d(v_3 = 0) = 0.05\,|c_d(v_3 = 0)|$. The comparison between theoretical and observed spectra is very satisfactory but is only qualitative: the calibration of this early recording did not really enable us to measure precise splittings in the spectrum. We must also point out that we could not determine the sign of c_d from this cluster and a very similar synthetic spectrum can be drawn with $c_d(v_3 = 0) = -4.25$ kHz and the same Δc_d. The sign of c_d will be determined in the following example. Finally one can notice that the intensities of F_1^{10} and F_2^{10} lines are not equal, as one would predict from the nuclear statistical weights; this is understandable because lines involving levels which are perturbed by the mixings lose much of their intensities which go as the fourth power of the coefficients of the eigenvectors. Furthermore the presence of crossovers modifies the observed intensities. A typical example of this phenomenon is shown in fig. 9: the P(84) $A_2^1F_2^3F_1^3A_1^1$ cluster is very tight (830 kHz wide) and, because of the important hyperfine mixings, the nuclear statistic intensity ratio of 10 to 6 between A_2 and F lines is not observed. The observed intensity ratio is well reproduced theoretically; this shows that in such a case a superfine fit alone cannot be worked out satisfactorily, though only superfine splittings are observed, and that one needs the hyperfine operators to give a correct account of the intensities.

(D) P(4)

The P(4) manifold is made of the four lines $A_1F_1EF_2$ which do not form a cluster and spread over 60 MHz; only the lines A_1F_1E could be reached with our waveguide laser and can be seen in fig. 11. Crossovers are observed between A_1 and F_1, between A_1 and E and between F_1 and E. They arise because the coupled basis functions are indeed strongly mixed in the ground state: to give an idea, the eigenvectors of the $(F = 4)$g subblock have components of the order of 0.75, 0.60, 0.10 and 0.25 in the basis $|0, 4, 4, A_{1g}, 0,4\rangle$, $|0, 4, 4, F_{2g}, 2, 4\rangle$, $|0, 4, 4, F_{2g}, 0, 4\rangle$ and

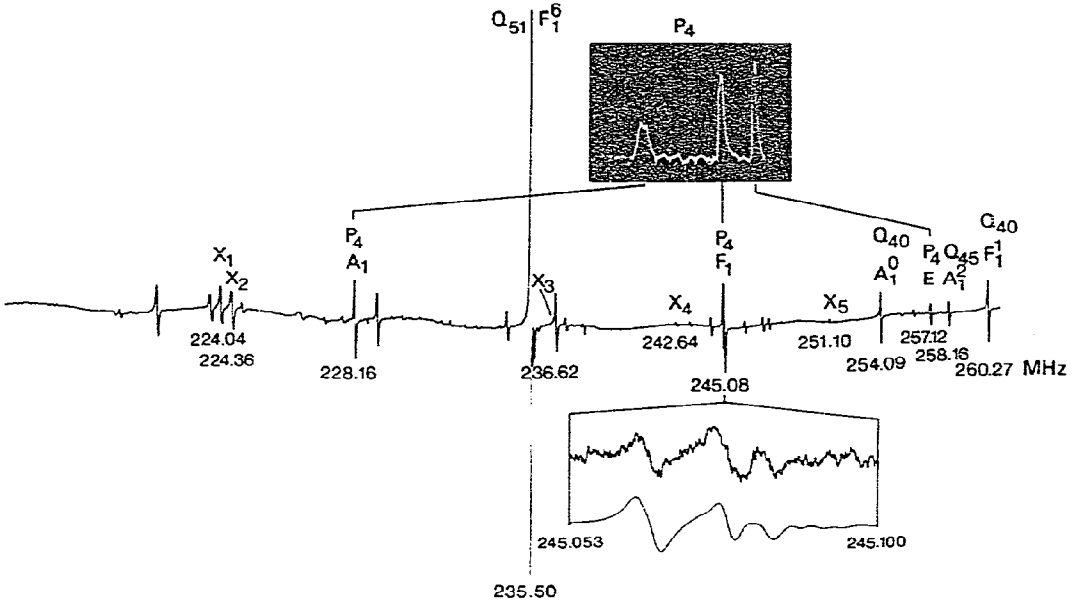

Fig. 11. Part of the P(4) manifold. Top: supersonic beam spectrum with bolometric detection [40]. Middle: saturation spectrum obtained with a free-running waveguide laser in a room-temperature cell (detunings are in MHz from $Q(38)E^0$). Bottom: The $P(4)F_1$ component recorded with a frequency offset-locked waveguide laser is compared with a calculated spectrum (in the middle spectrum this line is blended with an unidentified F_2 line). Crossover resonances are labeled by Xs: X_1 and X_2 are crossovers belonging to the $Q(51)F_2^6F_1^6$ system; X_3, X_4 and X_5 are the P_4 crossovers respectively in the center of the $(A_1F_1)(A_1E)$ and (F_1E) intervals.

$|0, 4, 4, F_{1g}, 1, 4\rangle$. In the $\nu_3 = 0$ hamiltonian matrix, of dimension 22, only the four states with $F = J \pm 2$ are not mixed; in the $\nu_3 = 1$ matrix, eigenvectors with the same C_{VR} and different J are also substantially mixed: e.g. the two functions $|1, 3, 4, E, 2, 2\rangle$ and $|1, 3, 4, E, 1, 2\rangle$ are mixed with coefficients equal to 0.88 and 0.47. In this low-J example, the effects of spin–spin and spin–rotation operators are comparable in magnitude and diagonal matrix elements of tensor hyperfine interactions are comparable to off-diagonal ones. The effect of diagonal matrix elements of the tensor spin–rotation operator has been seen for the first time when we tried to reproduce the hyperfine structure of the $P(4)F_1$ line (fig. 11); these matrix elements are non-zero because the product of representations $F_1 \times F_1$ contains E; this fact enables us to choose the sign of c_d: the synthetic spectrum in fig. 11 is drawn with $c_d = +4.25$ kHz and $c_d(\nu_3 = 1) = 1.05\, c_d$. Again this Δc_d certainly stems from the tensor spin–vibration interaction but we wait for the analysis of more structures to derive a tensor spin–vibration coupling constant from our effective Δc_d. Indeed what happens, hidden in the three lines of fig. 11, is more complicated than just three hyperfine components with $F = J, J \pm 1$: first F_{1g} and F_{1u} components are well split, second, owing to the mixings, some cross-overs and forbidden lines are strong so that the spectrum is made up of 16 non-negligible lines (whose frequencies and intensities are sensitive to almost all constants) and one should not be abused by the simplicity of three observed lines. In the final example to come, the splitting of a vibration–rotation line into hyperfine components reflects much more closely the decomposition of J into F.

(E) $R(28)A_2^0$ (fig. 1)

This line belongs to the trigonal cluster $A_2^0F_2^1F_1^1A_1^0$, but, in this J-manifold the clusterization moves rapidly to tetragonal clusters: the lines next to our cluster are $F_2^2 + E^1$ [4] (which is neither a trigonal nor a tetragonal cluster) and are not that far; so, we have added the E^1 states to our basis and, as in P(4), we do not work within a Harter's cluster. Finally, the only states that can strongly interact are E^1, A_2^0 and F_1^1; this leads to two 21 × 21 matrices. In the synthetic spectrum of this same line reported in ref. [2] (as well as for the two other A_2 lines in P(33) and P(59) manifolds [2,9]) no matrix had been diagonalized since only scalar hyperfine operators had been used; however, with the improved resolution of fig. 1, off-diagonal terms are needed to fit the spectrum; the only lines which are not affected by diagonalization are the extreme left and right lines since only A_2 vibration–rotation states can be associated with $I = 3$ and exhibit subcomponents with $F = J \pm 3$; all the other hyperfine components are shifted by a different amount for each component. Evidence of that fact appears in the spectrum of fig. 1: without tensor hyperfine interactions the three splittings of $[(A_2, I = 1, F), (A_2, I = 3, F)]$ doublets are identical (and equal to 0.8 kHz); the additional splittings due to tensor interactions are 0.8 kHz for $F = 27$ and 29 but only 0.3 kHz for $F = 28$. The details of the contribution to these additional splittings show that the role played by the E^1 vibration–rotation state which does not belong to the cluster is as important as the role played by the F_2^1 state which does belong to the cluster.

5. Conclusion

As a conclusion, let us point out that, if the various patterns of superfine clusters displayed in this paper confirm and illustrate the tunneling structures associated with internal tumbling motions, we have also shown the impossibility to consider separately superfine and hyperfine structures in an actual molecule. We have limited this demonstration to cases where only the ground level has hyperfine splittings comparable to or larger than the superfine structure but our approach applies equally well to cases where a diagonalization is required in both states (e.g. $R(29)F_1^2$–F_2^1 in fig. 1). Among the numerous spectra recorded recently at very high resolution (≈kHz) with waveguide CO_2 lasers and which have not yet been analysed, there is a large number of lines for which both levels correspond to the limit case 2 of Harter and Patterson and which exhibit so-called "superhyperfine" structures [38].

The present paper is to be considered as a preliminary account of a larger piece of work that should keep us busy for the next few years: a systematic, detailed analysis of all the spectra now available in order to provide a complete understanding of the internal dynamics of nuclear spins interacting together or with the molecular field within a rotating and vibrating molecule. The large number of spectral structures which have to be reproduced with a rather limited number of

hyperfine and fine structure constants is a stringent test of internal consistency. The introduction of new terms in the hyperfine hamiltonian might be required but in any case the only rigorous way to achieve this program is to perform the diagonalization of large enough hamiltonian matrices with a unique set of molecular constants as described in this paper.

Note added in proof

Allowing for a much wider range of possible values for Δc_d we have recently obtained a substantially improved fit for the P(4) F_1 line with a negative c_d = −4.25 kHz and a $\Delta c_d \simeq 3$ kHz. Such a large Δc_d is consistent with the Δc_d used for P(82) and the relationship between a unique constant X and the parameters Δc_d. Calculated and observed intensities are now in good agreement, which is not the case in fig. 11. A new figure will be published in a future addendum to this paper.

Acknowledgement

The authors would like to thank Drs. G. Tarrago and G. Poussigue who provided them with the values of off-diagonal isoscalar K coefficients. They are also grateful to Dr. F. Michelot and Professor W.G. Harter for critically reading the manuscript.

Appendix: Relevant numerical values

A.1. Hamiltonian constants

t_{044} = 5.7 Hz [12], t_{244} = 1125.58 kHz [2],

c_a = −5.27 kHz [41], c_d = 4.25 kHz .

To be consistent with the definition of c_d given in eq. (13), one must take half the value given in ref. [12]. The sign of c_d is determined from the recent observation of the P(4)F_1 line shown in fig. 11.

d_1 = 9.82 kHz [41], d_2 = 3.47 kHz [41],

A = 4.4 kHz [2].

A.2. Off-diagonal isoscalar coefficients [42]

These coefficients satisfy the relationship:

$$K^{J_1\ J_2\ J_3}_{n_1C_1\ n_2C_2\ n_3C_3} = (-1)^{J_1+J_2+J_3+C_1+C_2+C_3} \times K^{J_2\ J_1\ J_3}_{n_2C_2\ n_1C_1\ n_3C_3} .$$

We shall write $K^{J\ \ 2\ \ J}_{n_1C_1\ C\ n_2C_2}$ as $K(J, n_1C_1, C, n_2C_2)$.

$K(53, 6F_1, E, 6F_1) = -0.05$,
$K(53, 6F_1, E, 6F_2) = 0.08$,
$K(53, 6F_2, E, 6F_2) = -0.05$,

$K(53, 6F_1, F_2, 6F_1) = -0.003$,
$K(53, 6F_1, F_2, 6F_2) = -0.001$,
$K(53, 6F_2, F_2, 6F_2) = -0.0008$,

$K(38, 0F_2, E, 0F_1) = -0.000064$,
$K(38, 0F_1, E, 0F_1) = 0.000069$,
$K(38, 0F_2, E, 0F_2) = -0.000069$,
$K(38, 0E, E, 0E) = 0.00023$,

$K(38, 0F_2, F_2, 0F_2) = -0.08$,
$K(38, 0E, F_2, 0F_1) = -0.1$,
$K(38, 0F_1, F_2, 0F_1) = 0.08$,
$K(38, 0F_1, F_2, 0F_2) = -0.13$,

$K(54, 2A_2, E, 4E) = 0.054$,
$K(54, 4E, E, 4E) = 0.054$,

$K(4, E, E, E) = -0.14$,
$K(4, F_1, E, F_1) = -0.41$,
$K(4, F_2, E, F_2) = 0.12$,
$K(4, A_1, E, E) = 0.28$,
$K(4, F_1, E, F_2) = 0.14$,

$K(4, F_1, F_2, F_1) = -0.13$,
$K(4, F_2, F_2, F_2) = 0.23$,
$K(4, A_1, F_2, F_2) = 0.17$,
$K(4, E, F_2, F_1) = 0.14$,
$K(4, E, F_2, F_2) = 0.32$,
$K(4, F_1, F_2, F_2) = 0.33$,

$K(28, 1E, E, 0A_2) = 0.04$,
$K(28, 1E, E, 1E) = 0.06$,
$K(28, 1F_1, E, 1F_1) = -0.010$,

$K(28, 0A_2, F_2, 1F_1) = 0.10$,
$K(28, 1E, F_2, 1F_1) = -0.018$,
$K(28, 1F_1, F_2, 1F_1) = -0.16$.

References

[1] J.L. Hall and Ch.J. Bordé, Phys. Rev. Letters 30 (1973) 1101;
Ch.J. Bordé and J.L. Hall, in: Laser spectroscopy, eds. R.G. Brewer and A. Mooradian (Plenum Press, New York, 1974) p. 125;
J.L. Hall, Ch.J. Bordé and K. Uehara, Phys. Rev. Letters 37 (1976) 1339.

[2] Ch.J. Bordé, M. Ouhayoun, A. van Lerberghe, Ch. Salomon, S. Avrillier, C.D. Cantrell and J. Bordé, in: Laser spectroscopy IV, eds. H. Walther and K.W. Rothe (Springer, Berlin, 1979) p. 142.

[3] H. Brunet and M. Perez, J. Mol. Spectry. 29 (1969) 472.

[4] R.S. McDowell, H.W. Galbraith, B.J. Krohn, C.D. Cantrell and E.D. Hinkley, Opt. Commun. 17 (1976) 178;
R.S. McDowell, H.W. Galbraith, C.D. Cantrell, N.G. Nereson and E.D. Hinkley, J. Mol. Spectry. 68 (1977) 288.

[5] Ch.J. Bordé, Compt. Rend. Acad. Sci. (Paris) 271B (1970) 371; Post-deadline paper 22.7P, VIth International Quantum Electronics Conference, Kyoto (1970).

[6] M. Ouhayoun and Ch.J. Bordé, Metrologia 13 (1977) 149.

[7] A. van Lerberghe, S. Avrillier and Ch.J. Bordé, IEEE J. Quantum Electron. QE-14 (1978) 481.

[8] A. van Lerberghe, S. Avrillier, Ch.J. Bordé and C.D. Cantrell, J. Opt. Soc. Am. 68 (1978) 624.

[9] Ch.J. Bordé, M. Ouhayoun and J. Bordé, J. Mol. Spectry. 73 (1978) 344.

[10] Ch. Salomon, Ch. Breant, Ch.J. Bordé and R.L. Barger, J. Phys. (Paris) 42, Suppl. to no. 12 (1981) C8-3.

[11] A. Clairon, A. van Lerberghe, Ch. Salomon, M. Ouhayoun and Ch.J. Bordé, Opt. Commun. 35 (1980) 368;
A. Clairon, A. van Lerberghe, Ch. Breant, Ch. Salomon, G. Camy and Ch.J. Bordé, J. Phys. (Paris) 42, Suppl. to no. 12 (1981) C8-127.

[12] J. Bordé, Ch.J. Bordé, Ch. Salomon, A. van Lerberghe, M. Ouhayoun and C.D. Cantrell, Phys. Rev. Letters 45 (1980) 14.

[13] Ch. Breant, Ch. Salomon, A. van Lerberghe, G. Camy and Ch.J. Bordé, Appl. Phys. B (1982), to be published.

[14] W.G. Harter and C.W. Patterson, J. Chem. Phys. 66 (1977) 4872, 4886.

[15] A.J. Dorney and J.K.G. Watson, J. Mol. Spectry. 42 (1972) 135.

[16] W.M. Itano, J. Mol. Spectry. 71 (1978) 193.

[17] F. Michelot, B. Bobin and J. Moret-Bailly, J. Mol. Spectry. 76 (1979) 374.

[18] A. Dymanus, in: Physical chemistry, Series Two, Vol. 3, ed. D.A. Ramsay (Butterworths, London, 1976) p. 127.

[19] J.-C. Hilico, H. Berger and M. Loete, Can. J. Phys. 54 (1976) 1702.

[20] J.D. Louck and H.W. Galbraith, Rev. Mod. Phys. 48 (1976) 69.

[21] J.-P. Champion, G. Pierre, F. Michelot and J. Moret-Bailly, Can. J. Phys. 55 (1977) 512.

[22] F. Michelot, J. Mol. Spectry. 63 (1976) 227.

[23] J.S. Griffith, The irreducible tensor method for molecular symmetry groups (Prentice-Hall, Englewood Cliffs, 1962).

[24] J. Moret-Bailly, L. Gautier and J. Montagutelli, J. Mol. Spectry. 15 (1965) 355.

[25] B.R. Judd, Angular momentum theory for diatomic molecules (Academic Press, New York, 1975).

[26] J. Bordé, J. Phys. (Paris) 12 (1978) L-175.

[27] H. Berger, J. Phys. (Paris) 38 (1977) 1371.

[28] J. Moret-Bailly, Cahiers Phys. 15 (1961) 237.

[29] K.T. Hecht, J. Mol. Spectry. 5 (1960) 355.

[30] F. Michelot, Thesis, University of Dijon, France (1980).

[31] J.-C. Hilico, J. Phys. (Paris) 31 (1970) 15.

[32] A. Robiette, D.L. Gray and F.W. Birss, Mol. Phys. 32 (1976) 1591.

[33] B. Krohn, Los Alamos Scientific Laboratory report, LA-6554 MS (1976).

[34] P.N. Yi, I. Ozier and C.H. Anderson, Phys. Rev. 165 (1968) 92.

[35] R.L. Cook and F.C. de Lucia, Am. J. Phys. 39 (1971) 1433.

[36] K. Uehara and K. Shimoda, J. Phys. Soc. Japan 36 (1974) 542.

[37] J. Bordé and Ch.J. Bordé, J. Mol. Spectry. 78 (1979) 353.

[38] W.G. Harter, Phys. Rev. A24 (1981) 192.

[39] H. Berger and A. Aboumajd, J. Phys. 42 (1981) L-55.

[40] S. Avrillier, J.M. Raimond, Ch.J. Bordé, D. Bassi and G. Scoles, Opt. Commun. 39 (1981) 311;
Ch.J. Bordé, S. Avrillier, A. van Lerberghe, Ch. Salomon, D. Bassi and G. Scoles, J. Phys. (Paris) 42, Suppl. no. 12 (1981) C8-15.

[41] I. Ozier, P.N. Yi and N.F. Ramsey, J. Chem. Phys. 66 (1977) 143.

[42] G. Poussigue and G. Tarrago, private communication.

[43] W.G. Harter, C.W. Patterson and F.J. da Paixao, Rev. Mod. Phys. 50 (1978) 37.

[44] W.G. Harter and C.W. Patterson, Phys. Rev. A19 (1979) 2277.